UNIVERSIDAD DE INVESTIGACIÓN DE TECNOLOGÍA EXPERIMENTAL YACHAY

Escuela de Ciencias Biológicas e Ingeniería

TÍTULO: ELECTRICAL CHARACTERIZATION OF FLEXIBLEECG PATCH

Trabajo de integración curricular presentado como requisito parala obtención del título de Ingeniera Biomédica

Autor:

Nataly Sabina Milán Cucurí

Tutor:

Almeida Galárraga, Diego Alfonso, Ph.D.

Urcuquí, 26 de septiembre de 2022

SECRETARÍA GENERAL
ESCUELA DE CIENCIAS BIOLÓGICAS E INGENIERÍA
CARRERA DE BIOMEDICINA
ACTA DE DEFENSA No. UITEY-BIO-2022-00028-AD

En la ciudad de San Miguel de Urcuquí, Provincia de Imbabura, a los 26 días del mes de septiembre de 2022, a las 13:30 horas, en el Aula S_CAN de la Universidad de Investigación de Tecnología Experimental Yachay y ante el Tribunal Calificador, integrado por los docentes:

Presidente Tribunal de Defensa	Mgs. VILLALBA MENESES, GANDHI FERNANDO
Miembro No Tutor	CRUZ VARELA, JONATHAN DAVID
Tutor	Dr. ALMEIDA GALARRAGA, DIEGO ALFONSO , Ph.D.

Se presenta el(la) señor(ita) estudiante **MILAN CUCURI, NATALY SABINA**, con cédula de identidad No. **0604305003**, de la **ESCUELA DE CIENCIAS BIOLÓGICAS E INGENIERÍA**, de la Carrera de **BIOMEDICINA**, aprobada por el Consejo de Educación Superior (CES), mediante Resolución **RPC-SO-43-No.496-2014**, con el objeto de rendir la sustentación de su trabajo de titulación denominado: **Electrical characterization of flexible ECG patch** , previa a la obtención del título de **INGENIERO/A BIOMÉDICO/A**.

El citado trabajo de titulación, fue debidamente aprobado por el(los) docente(s):

Tutor	Dr. ALMEIDA GALARRAGA, DIEGO ALFONSO , Ph.D.

Y recibió las observaciones de los otros miembros del Tribunal Calificador, las mismas que han sido incorporadas por el(la) estudiante.

Previamente cumplidos los requisitos legales y reglamentarios, el trabajo de titulación fue sustentado por el(la) estudiante y examinado por los miembros del Tribunal Calificador. Escuchada la sustentación del trabajo de titulación, que integró la exposición de el(la) estudiante sobre el contenido de la misma y las preguntas formuladas por los miembros del Tribunal, se califica la sustentación del trabajo de titulación con las siguientes calificaciones:

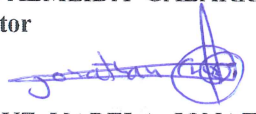| Tipo	Docente	Calificación
Miembro Tribunal De Defensa	CRUZ VARELA, JONATHAN DAVID	10,0
Presidente Tribunal De Defensa	Mgs. VILLALBA MENESES, GANDHI FERNANDO	10,0
Tutor	Dr. ALMEIDA GALARRAGA, DIEGO ALFONSO , Ph.D.	10,0

Lo que da un promedio de: **10 (Diez punto Cero)**, sobre 10 (diez), equivalente a: **APROBADO**

Para constancia de lo actuado, firman los miembros del Tribunal Calificador, el/la estudiante y el/la secretario ad-hoc.

MILAN CUCURI, NATALY SABINA
Estudiante

Mgs. VILLALBA MENESES, GANDHI FERNANDO
Presidente Tribunal de Defensa

Dr. ALMEIDA GALARRAGA, DIEGO ALFONSO , Ph.D.
Tutor

CRUZ VARELA, JONATHAN DAVID
Miembro No Tutor

ALARCON FELIX, KARLA ESTEFANIA
Secretario Ad-hoc

Autoría

Yo, **Nataly Sabina Milán Cucurí**, con cédula de identidad **0604305003**, declaro que las ideas, juicios, valoraciones, interpretaciones, consultas bibliográficas, definiciones y conceptualizaciones expuestas en el presente trabajo; así cómo, los procedimientos y herramientas utilizadas en la investigación, son de absoluta responsabilidad de él/la autor(a) del trabajo de integración curricular. Así mismo, me acojo a los reglamentos internos de la Universidad de Investigación de Tecnología Experimental Yachay.

Urcuquí, Septiembre del 2022.

Nataly Sabina Milán Cucurí
CI: 0604305003

Autorización de publicación

Yo, **Nataly Sabina Milán Cucurí**, con cédula de identidad **0604305003**, cedo a la Universidad de Tecnología Experimental Yachay, los derechos de publicación de la presente obra, sin que deba haber un reconocimiento económico por este concepto. Declaro además que el texto del presente trabajo de titulación no podrá ser cedido a ninguna empresa editorial para su publicación u otros fines, sin contar previamente con la autorización escrita de la Universidad.

Asimismo, autorizo a la Universidad que realice la digitalización y publicación de este trabajo de integración curricular en el repositorio virtual, de conformidad a lo dispuesto en el Art. 144 de la Ley Orgánica de Educación Superior.

Urcuquí, Septiembre del 2022.

Nataly Sabina Milán Cucurí
CI: 0604305003

Dedication

"To my grandparents, Mama Ramona, Mama Goya, and Papa Fico, for always motivating me to pursue my dreams. This thesis is the product of your prayers: to be focus on my studies, dream big, and that with work and effort, I can achieve everything I set out to do. Thank you for trusting me and for the unconditional love that all of you give me."

Acknowledgments

Abstract

Recording electrical activity is essential to monitor organs such as the heart. It is of the utmost importance to obtain a good quality cardiac signal for medical follow-up and to achieve a better diagnosis of cardiac problems. Currently, wet or commercial Ag/AgCl electrodes are openly accepted in the clinical setting, obtaining a good cardiac signal; however, they present adversities, such as abrasion, allergy, and skin irritation, due to the gel used. Therefore, in recent years, research on dry electrodes has been developed to solve these adversities and put aside the use of gels. However, dry electrodes still have a higher impedance than wet electrodes and are more expensive to produce. 3D printing - an alternative manufacturing method - is faster and lowers costs due to the minimal use of material resources. 3D printing opens up a world of possibilities for creating custom sensors. In this thesis, 3D electrodes based on a conductive material were printed to measure resistance, skin impedance and obtain the cardiac signal. Additionally, the 3D printing conditions and the skin preparation were evaluated during the measurements.

Keywords: Dry electrodes, ECG, skin impedance, 3D printing, conductive material.

Resumen

El registro de la actividad eléctrica es fundamental para monitorear órganos como el corazón. Es de suma importancia obtener una buena calidad de señal cardíaca para el seguimiento médico y lograr un mejor diagnóstico de los problemas cardíacos. Actualmente, los electrodos húmedos o comerciales de Ag/AgCl son aceptados abiertamente en el ámbito clínico, obteniendo una buena señal cardiaca; sin embargo, presenta adversidades como abrasión, alergia e irritación de la piel, debido al gel utilizado. Por tanto, en los últimos años se ha desarrollado la investigación de electrodos secos para solventar estas adversidades y dejar de lado el uso de geles. No obstante, los electrodos secos aún presentan una impedancia mayor que los electrodos húmedos, además de ser más costosos en su producción. La impresión 3D -un método alternativo de fabricación- es más rápido y reduce costos debido al uso mínimo de recurso material. La impresión 3D abre un mundo de posibilidades para crear sensores personalizados. En esta tesis se imprimió electrodos 3D basados en un material conductivo para la medición de resistencia, impedancia de la piel y obtención de la señal cardiaca. Adicionalmente, se evaluó tanto las condiciones de impresión 3D como la preparación de la piel durante las mediciones.

> ***Palabras Clave***: Electrodos secos, ECG, electrocardiograma, impedancia de la piel, impresión 3D, material conductivo.

Contents

List of Tables

List of Figures

List of Equations

Abbreviations

3D   Three-Dimensional

Ca^{2+} Calsium Ion

K^+ Potassium Ion

Na^+ Sodium Ion

ABS   Acrylonitrile Butadiene Styrene

Ag   Silver

AgCl   Silver Chloride

AHA   American Heart Association

AM   Additive Manufacturing

ASTM American Society for Testing and Materials

Au   Gold

CAD   Computer-Aided Design

Cu   Copper

DC   Direct Current

DIM   Direct Ink Writing

ECG   Electrocardiography

EEG   Electroencephalography

EEG   Electromyogram

EIS   Electrochemical Impedance Spectroscopy

EOG   Electrooculogram

FDM   Fused Deposition Modeling

IEC   International Electrotechnical Commission

IMFs Ion Motive Forces

LIO   Leech-Inspired Origami

MP   Membrane Potential

MWCNT Multi-Wallet Carbon Naanotube

Ni   Nickel

PCL   PolyCaproLactone

PDMS PolyDiMethylSiloxane

PE   Printed Electronics

PET   PolyEthyleneTerephthalate

PETG PolyEthylene Terephthalate Glycolized

PLA   PolyLactic Acid

PVA   PolyVinyl Alcohol

SEM   Scanning Electron Microscope

STL   STereoLithography

Chapter 1

Introduction

This chapter describes the background of printed electronics and the type of manufacturing that is 3D printing. In addition to the problem statement for which this thesis has been developed, it also describes the general and specific objectives with which the conclusions will be obtained at the end of this thesis. Finally, an outline of each chapter developed in this writing is shown.

1.1 Background

Printed Electronics (PE) has emerged as a revolutionizing of how electronics are fabricated, becoming more popular in industry and academia [7]. Areas such as electronics, packaging, Internet of Things, and biomedicine have been favored [22, 23]. Contrary to the conventional microelectronics process based on subtractive manufacturing techniques, PE is based on the additive deposition of functional materials like piezoelectric ones [22, 24]. Therefore, PE can manufacture high-quality electronic products with features like thin, flexible, wearable, lightweight, of varying sizes, ultra-cost-effective, and environmentally friendly [23, 25, 13, 17]. Under this method, it's possible to print electronic circuits, interconnects, electrical components, and devices [22].

Additive manufacturing (AM) is a technology with which it is possible to innovate in a revolutionary way and apply it in the medical field [26, 27, 25]. Some of them are the tissue and organ fabrication in the biomedicine field and the creation of customized prosthetics and printing wearable devices in the bioengineering field [28, 29]. Nowadays, researchers have explored the 3D printing of biosensing platforms such as glucose sensors, sweat sensors, artificial skin, electroencephalography (EEG) , electrocardiography (ECG), etc [29].

According to the American Society for Testing and Materials (ASTM) , photopolymerization, powder bed fusion, binder jetting, material jetting, material extrusion, sheet lamination, and directed energy deposition are the seven main categories of 3D printing technology [29, 30]. The categorization is based on the method of material deposition and working principle [29]. In addition, the need to use a different material for different types of the sensor has been open the market for multiple materials such as conductors,

dielectrics, flexible and still ones [31]. During the development of the thesis, the material extrusion technology and a flexible conductive material will be used to aims its potential as dry electrode for ECG.

1.2   Problem statement

The electrocardiography is an efficient technique and accepted clinical practice used to monitor the heart directly by providing a representation of the electrical activity [32, 23]. It has to acquired the ECG signal through the patient module [32] and due to surface ECG is a low amplitude signal recorded in the presence of a significant interference, its important to have a careful attention to factors as skin preparation and electrode adhesion to reduce artifact and interference [32].

Silver/silver chloride (Ag/AgCl) bioelectrode is the most commonly used for ECG [33], however, present some disadvantages like the disposable electrodes has to be replace after several hours of usage to avoid skin irritation and allergic contact dermatitis [32, 34]. Also, patient has to be repeating dry shaving with blade showing a skin abrasion. Therefore, attention to patient comfort and biocompatibility are very important factors for researches whom seek new alternatives to overcome these problems but with the same diagnostic efficiency [32, 23].

Therefore, more research on new forms to obtain the heart signal has been done in the last decade. Dry electrodes that do not operate with the need for a gel or abrasive skin preparation have been developed to overcome difficulties mentioned for gel electrodes [23, 35, 5]. However, researchers still focus on solving the gel electrodes problematic without reducing signal quality. Thus, study new conductive materials and new processes to develop them to guarantee comfort properties and high-quality signals obtention, which is the main aim of the recent work of producing dry electrodes [5]. For these reasons, we decided to use a new filament with highly conductivity -compared with filaments on marked- [36] used for develop dry electrodes and research its potential the signal recognition during ECG.

1.3   Objectives

1.3.1   General Objective

Electrical characterization of flexible dry electrodes created from 3D printing with a specific conductive filament and its potential as a cardiac electrode.

1.3.2   Specific Objectives

- Design and 3D printing of dry flexible flat electrodes with the Electrifi filament.

- Resistivity and impedance test to 3D printed dry flexible flat electrodes based on printing parameters and morphology.

- Impedance Frequency response over skin of the 3D printed dry flexible flat electrodes.

- Cardiac signal acquisition using the 3D printed dry flexible flat electrodes.

1.4   Outline

In this thesis, several concepts related to the development of electrodes focused on the acquisition of bioimpedance and cardiac signals were covered. Chapter 1 introduces background on 3D printing and how this form of additive manufacturing has been submitted to the medical field and, in the case of the thesis topic, in the creation of electrodes. Likewise, the problem statement about silver/silver chloride electrodes is mentioned, which are the most used in the medical field, and the importance of solving the problems of commercial electrodes. Finally, the objectives for the development of this project are presented. Chapter 2 presents the theoretical framework where what is necessary to understand the acquisition of bioimpedance and the ECG signal waveform is exposed; it is mentioned the biological and anatomical process related to bioelectric signal and the heart; it is mentioned what an electrode is, its type, and its electrical operation. The materials used, their importance in 3D printing, and an understanding of the parameters necessary to develop the electrode. Chapter 3 presents the state of the art of dry electrodes developed in the last decade under 3D printing, and its results (bioimpedance and bioelectrical cardiac signal acquisition) are exposed. Chapter 4 describes the materials used throughout the methodology to develop dry electrodes and perform the measurements. Chapter 5 shows the results related to electrode design, resistance, electrode-skin impedance, and cardiac signal acquisition compared to commercial electrodes. Chapter 6, shows the discussion section comparing the results obtained with the literature. Finally, in Chapter 7, this thesis concludes with a discussion of the project's results and future research directions.

Chapter 2

Theoretical Framework

This chapter presents the necessary theory for understanding this thesis. First, it will present about the bioelectrical regarding the ECG and its regarding abouth the physiological capture of the heart signal. Secondly, it will be present the definition and properties of the medical electrodes. Thirdly, the conductive materials and how its the process of 3D printing. Finally, the electrical characterization and the formulas regarding the resistance, resistivity and impedance.

2.1 Bioelectrical signals

Physiological signals and basic ones of the human body where the most studied are the electrocardiogram (ECG), electroencephalogram (EEG) , electromyogram (EMG), and electrooculogram (EOG) [6].

Biological Cell

The partitioning of charged ions and molecules gives rise to electrical and chemical potential differences across cell membranes and electrochemical gradients or ion motive forces (IMFs) [1]. A membrane potential (MP) arises from the combined electrical potential differences across a given membrane due to all the charged molecules. The chemiosmotic theory of respiration is based on the maintenance of MP and the coupling of IMFs to membrane-bound chemical reactions, which are paramount for bioenergetics and cell physiology [37, 38]. However, these mechanisms differ depending on the membranes to be studied (mitochondrial membrane or plasma membrane) [39], involving processes known as electrostatic and electrodynamic [37].

Electrical Activity of the Myocardium

The electrical activity of the myocardium is attributed to the generation of action potentials of the cardiac cells and the coordinated electrical functioning of the entire heart; the surface electrocardiogram detects this [40]. Membrane potentials and ion movement in cardiac conducting cells are essential because of the differences between cardiac conducting cells
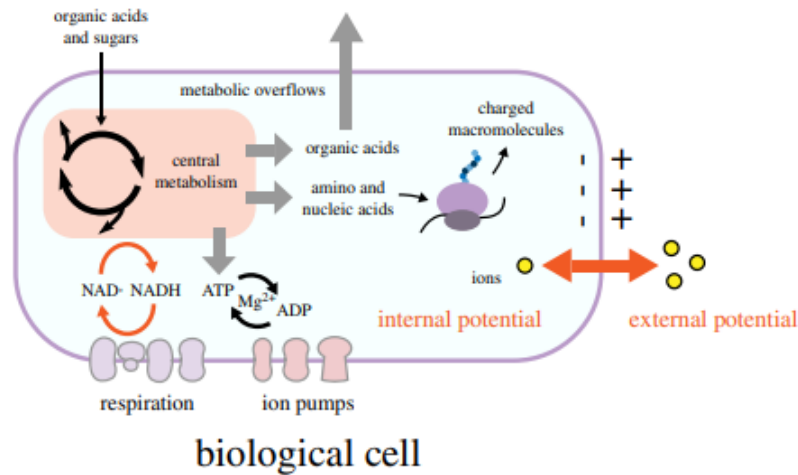
Figure 2.1: Bioelectrical view of cell, system rely on ion flox reactions across interfaces. Modified from [1]

and cardiac contractile cells since Na^+, K^+, and Ca^{2+} have key roles in both cell types [41]. Next, the operation for the movement of autorhythmicity properties of the heart muscle is explained. The membrane potential increases slowly for conducting cells from -60 mV to -40 mV approx due to the sodium ion channels involved. This movement creates a prepotential depolarization; Likewise, the opening of the calcium channels occurs, and the Ca^{2+} enters the cell, depolarizing it up to a value of approx +5 mV [42]. After reaching the value, the calcium ion channels close, and the potassium K^+ channels intervene by opening, giving the exit of K^+, and repolarization occurs. To the point that the potential reaches -60 mV, the K^+ channels close, the Na^+ channels open, and so on, the prepotential phase begins again [43],[44].
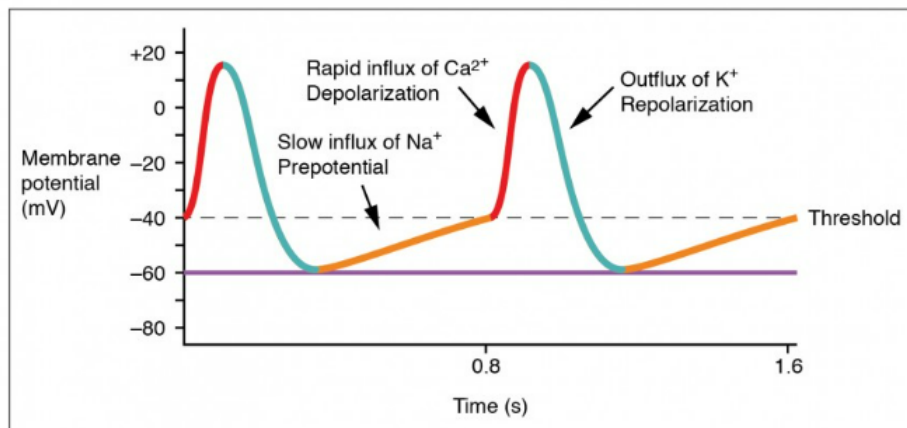
Figure 2.2: Membrane Potentials and Ion Movement in Cardiac Conductive Cells. Obtained from [2]

2.2   Heart

The heart is an organ that pumps blood throughout the body via the circulatory system. The heart contains four main sections or chambers made of muscle and powered by electrical impulses. In addition, its controls the rhythm and speed of the heart rate [3].
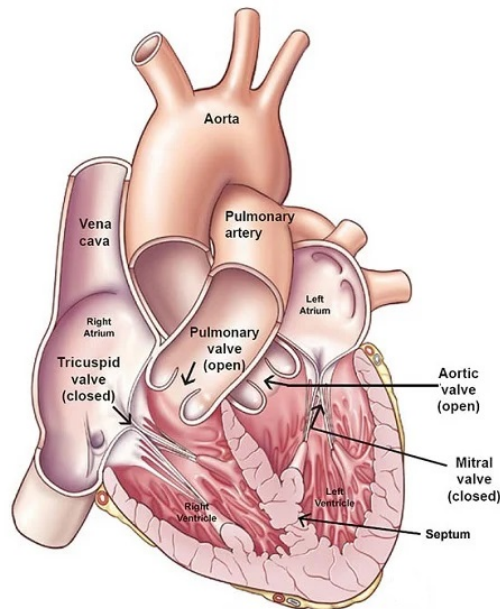
Figure 2.3: Heart's Overview. Obtained from [3]

2.2.1   Heart Rate

The heart rate is the number of times per minute the heart beats, which matches whatever happens in the person's environment or activity. This causes the heartbeat to get faster when the person is active and drops when the person is calm or resting. Likewise, the heart rate can be an important indicator of the overall health of people [45]. A good measure of heart rate is when it is subtracted. For most adults, the beats per minute (bpm) range between 60 and 100, considered a normal value [45]. This value can be affected by stress, medication, or how physically active the person is. If the value of resting heart rate is lower, it is better because it is related to high physical fitness, and the heart does not need to work as hard to maintain a steady beat [46].

2.3   Electrocardiogram

The electrocardiogram (ECG) is a noninvasive, easy and low cost test used to record the electrical activity of the heart using a set of electrodes placed in different parts of the body [47, 48, 49]. The signal obtained as a small difference in voltage between electrodes consequence of cardiac muscle depolarization and repolarization during each cardiac cycle.

Changes in the normal signal waveform occur in prescence of numerous cardiac abnormalities such as ventricular tachycardia [50], myocardial infarction [51, 52], and hyperkalemia [53].

2.3.1   ECG signal waveform

The ECG signal is characterized by five peaks known as fiducial points, represented by the letters P, Q, R, S, and T [54, 55]. The QRS complex is related with the depolarization of the right and left heart ventricles, this segment is known to be a reference point for signal analysis [55]. The P wave is the result of the depolarization of the atrium and the ventricle causes the rest of the peaks [4]. The figure 2.4 shows a schematic diagram of a human's heart normal sinus rhythm obtained by a ECG. The diagnosis of the signal depends on the morphology of the waves, and in addition the period of each peak and the segments that constitute. Therefore, detection of each section of the ECG signal is necessary for health professionals in diagnosis, screening, and monitoring of several heart conditions [56, 57].
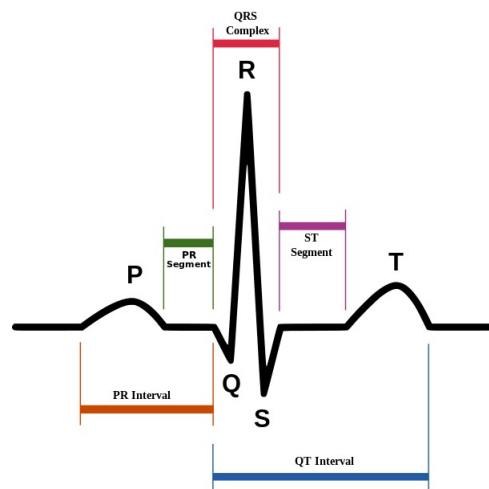
Figure 2.4: Schematic diagram of human's heart normal sinus rhythm. Obtained from [4]

2.3.2   Key Processes from ECG Monitoring

ECG monitoring fulfills a life cycle; they differ depending on the model and type of ECG; however, it is generalized in the following steps: data extraction and collection, preprocessing, feature extraction, processing and analysis, visualization, and support process [57].

ECG Data Acquisition

To acquire the information from the ECG monitoring system, some points have to be followed, such as (1) the type of sensor, whether wireless or wired, (2) the location of the sensors, (3) the number of sensors used and finally (4) the hardware to be used for monitoring, storage, and transmission [58, 57].

Preprocessing

Preprocessing is used to improve the quality of the raw signal, remove noise, and move the baseline wander and powerline interference [59, 60]. Specific attention must be paid to the acquired noise since it can come from powerline interference, baseline wander, electrode contact noise, electrode motion artifacts, and muscle contractions [57].

Feature Extraction

Feature extraction retrieves the most representative set of parameters from the preprocessor ECG and thus be used to characterize patterns. Some essential features like the area under the curve, peak amplitude, time delay between peaks and valleys, and heart rate frequency [57, 61, 62].

Processing and Analysis

Artificial intelligence and neural networks are used to interpret the electrocardiogram signals to discover diagnostic information, such as evaluating the quality and classification of the signal, detecting heartbeats, detecting peak and delay correction [57]. Several steps must be followed, such as signal amplification and its A/C conversion, noise elimination, and feature selection [63].

Visualization

In the ECG display, it can be managed under mobile or desktop applications where an environment is created with the user and interact with previously recorded ECG signals or in real-time [57]. Likewise, different ways of representing the cardiac signal can show mapping them, such as temporal, vectorial, spatial, and interactive [64].

Supporting Processes

As the name says, the support processes depend on the ECG monitoring system. They can have various functions such as signal selection process, data transfer [65], storage capacity reduction, data security, and privacy with encryption and decryption of the data [66] and the modeling and learning processes for the future work related to machine learning with the prediction and prognosis of diseases and in this case, cardiac ones [57].

2.3.3   ECG Lead Placement

The ECG waveform shape could change based on the location of the electrodes in the body since the potential register will change. The most widely used and accepted clinically is the 12-Lead ECG, where two color coding standards are used (American Heart Association (AHA) and International Electrotechnical Commission (IEC) system [67]; however, there are other standards such as 3-Lead and 5-Lead for ECG [68]. Likewise, there are different variations in the placement of the electrodes, for example, the Frank Lead Placement Sites, Mason-Likar and Cabrera 12-lead Placement Sites, or the Canadian Bipolar Chest Lead;

Each configuration or selected lead depends on the reason and ailments for performing the ECG [69].

2.4   Bioelectric electrodes

Electrodes are devices that convert the ionic potentials produced by the differents physiological procces in the human body into electronic potentials that can be interpreted by the differents electronic devices used in medicine [6, 5]. The electrodes used for mesure biosignals can be divided into wet, dry and capacitive electrodes [6]. The table 2.1 shows the advantages and 2.2 disadvantages of the mentioned electrodes in a summarized way.

Table 2.1: Advantages of bioelectric electrodes

Bioelectric electrodes	Advantages
Wet electrodes	Low cost, low polarization effect, low electrode-skin interface impedance and ease of use [6]
Dry electrodes	Long-term bioelectric monitoring on human surface, do not require skin pretreatment, do not require the application of conductive gel and stable skin contact interface [6]. (1) Penetrating contact: Higher electrical conductivity, similar impedance to wet electrodes and fewer motion artifacts (2) Non-penetrating contact: Suitable for hairy areas (3) Flat film dry electrodes: Flexibility and fits the contours of the skin (4) Textile dry electrode: Flexibility and moisture permeability [6, 5]
Capacitive electrodes	Do not require physical, conductive contact with the skin, do not trnasfer of charges and only displacement currents and more reliable and comfortable than other electrodes [6].

Table 2.2: Disadvantages of bioelectric electrodes

Bioelectric electrodes	Disadvantages
Wet electrodes	In long term: Need for skin pre-treatment, tendency to dry over time and skin irration [23, 6].
Dry electrodes	Higher noise levels from wet electrodes, higher impedance and costly. (1) Penetrating contact: Uncomfortable when piercing the skin and fracture of the microneedle electrodes. (2) Non-penetrating artifacts: Higher impedance than wet electrodes. (3) Flat film dry electrodes: Non-suitable for hairy sites. (4) Textile dry electrodes: Prone to relative slip, higher impedance than wet electrodes [5, 6]
Capacitive electrodes	Ultra-high impedance, instability at the electrode-skin interface, prone to noise, large discrepancy between the actual physiological signal and the human physiological signal [5, 6].

2.4.1 Wet Electrode

The most widely used electrode is the silver/silver chloride (Ag/AgCl) electrode. Also known as wet electrodes, use an electrolyte gel to form a conductive path between the skin and the electrode to reduce the impedance between the electrode and the skin. Nowadays, the wet electrodes are the current gold standard in clinical practice [70].

The following electrical equivalent circuit (Figure 2.5) can express the detection mechanism of the wet electrodes. It is shown how the electrodes represent an interface between the electrode charge transport of the ECG electrode and the ionic charge in the physical body, forming a half cell in the electrochemical electrode-electrolyte interface at the moment of contact between the electrode and the skin [5].

The Ehc refers to the half cell potential, the capacitor Cd and a resistor Rd in parallel as the interface structure. Rg refers to the gel's effective resistance, electrode, and skin. The skin structure comprises the stratum corneum, epidermis, and dermis-subcutaneous tissues where the difference between the ionic concentration in the stratum corneum creates the Es potential is created; the epidermis presents a circuit between resistance Re and capacitance Ce in parallel. Finally, the dermis and subcutaneous tissues (composed of blood vessels, nerves, preparatory glands, hair follicles) where their capacitance can be neglected and impedance can be treated as pure resistance Ru [5].
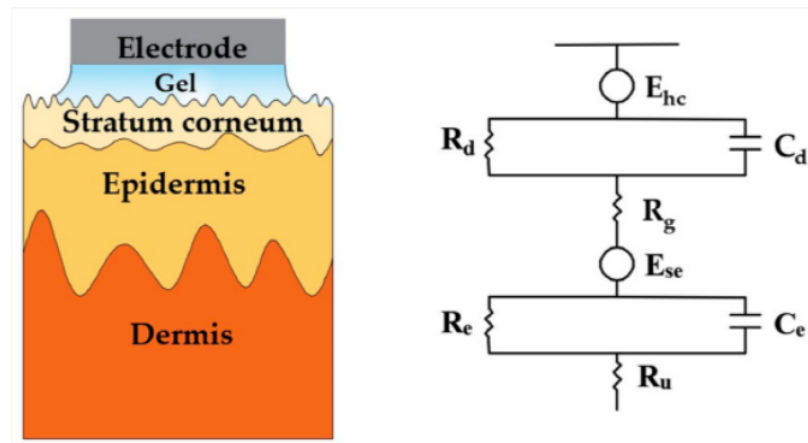
Figure 2.5: Electronic model of wet electrodes. Obtained from [5]

2.4.2 Surface Dry Electrode

Dry electrodes are noninvasive electrodes with closely contact to the skin, in contrast with conventional wet electrodes don't use conductive gels between the electrode and the skin surface [6]. They generally this electrodes have a higher impedance than wet electrodes but they won't cause any discomfort to the human body [6]. They can maintain a good contact with the skin, even during motion, beging suteable for use in ambulant applications such as health-care and to monitor exercise. It can represent the simplified electrical model for this electrodes as is Figure 2.6 where conductance Ci and resistance Ri are connected in parallel in exchange for the resistance Rg showed in the wet electrodes because the conductive gel is not used.
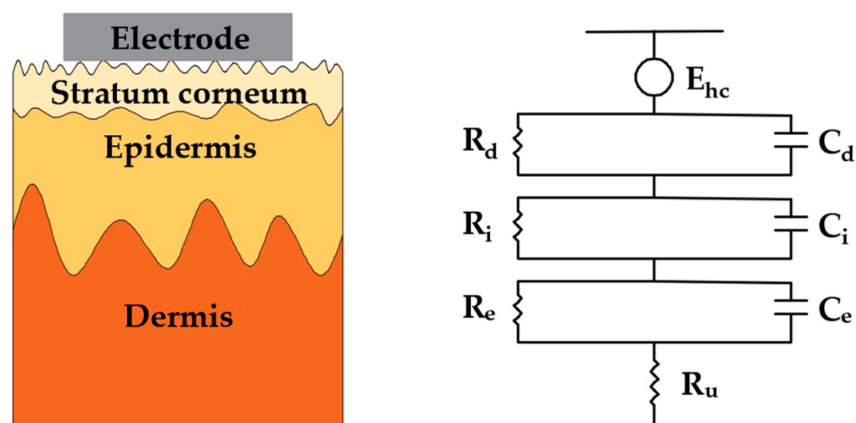
Figure 2.6: Electronic model dry electrodes. Obtained from [5]

2.4.3 Measurement principle of electrodes

The electrical activities from biological organisms during physiological activities are called bioelectrical phenomena, and can be recorded using a sensor call electrode. The electrodes

are usually placed on the epidermis where it is usually necessary to fix the electrode to the skin with an elastic band or medical tape [6].

To measure the signal, the electrodes are placed on the surface of the skin and placed in the area and position to be studied, in this case on the chest for heart measurement. Reference electrodes are used in an anatomical location that is considered to have a relatively stable biopotential together with the electrodes that will measure the electricity, additionally the ground electrodes are used to protect the noise interference when obtaining the signal [6].

The measurement principle is shown in Fig. 2.7, in the resting state, there is a potential difference between the inside and outside of the cell's membrane, with the outside and inside of membrane are positive and negative, respectively [44, 41]. Among them, the cell membrane is more permeable to K+, and K+ will diffuse outward with the concentration difference, which will cause part of the Na+ channel of the cell membrane to open when the cell is stimulated, and Na+ will flow inward with the concentration difference, which is positive inside the membrane and negative outside the membrane, thus creating a potential difference with the adjacent site and forming a local electric current that can be measured by a bioelectrical sensor [6, 41, 42].
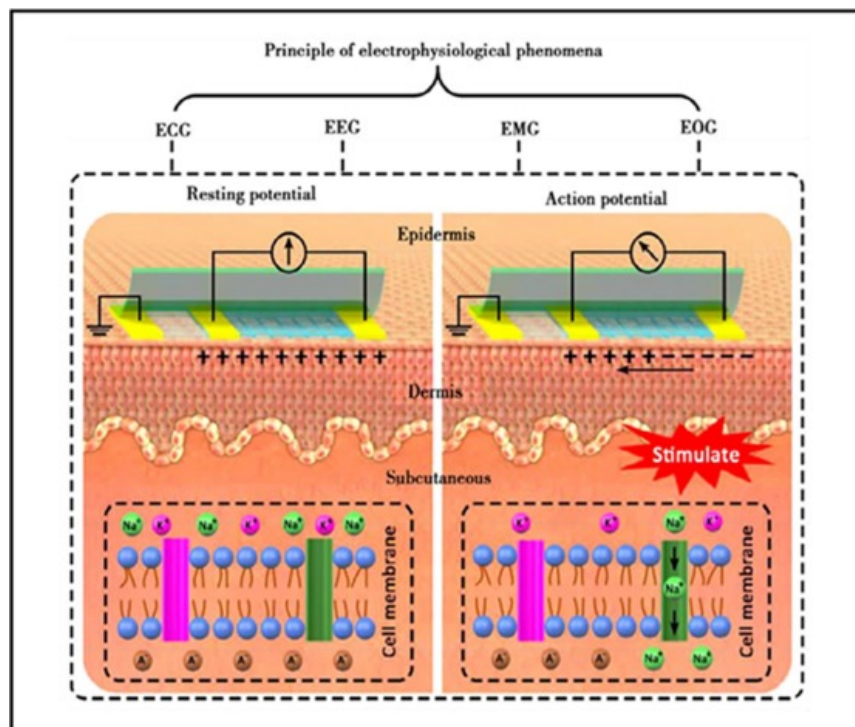
Figure 2.7: Principle of measurement of the electrodes. Obtained from [6]

2.5 3D printing

Also called additive manufacturing (Figure 2.9), it is known as fabricate three-dimensional physical objects from a geometric design known as computer-aided design (CAD) through the successive deposition of materials [7, 71, 72, 73].
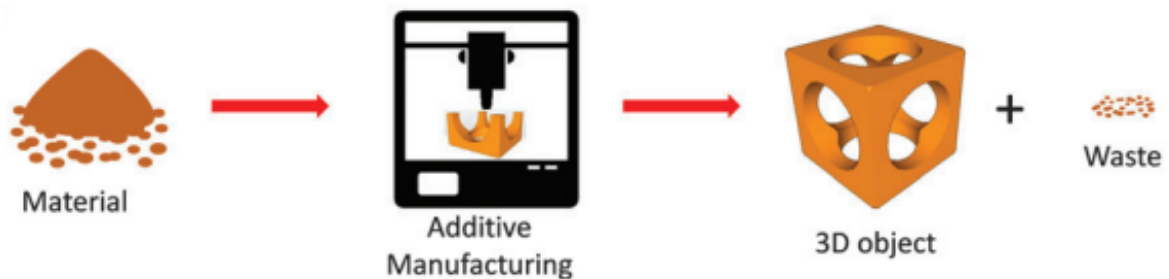
Figure 2.8: Additive manufacturing: A material is used by a 3D-printer depositing just the necessary amount of material layer-by-layer. In the end, the desired 3D object is obtained. Obtained from [7].

The steps to create an object with 3D printing are as follows. It starts with a design in computer-aided design software, a three-dimensional scanner, or photogrammetry. Once the 3D model is created, it is converted to an STL file format (from STereoLithography) which handles a list of coordinates of triangulated sections. Under the software of the 3D printer to be used, the information is converted to a G-code file, in which several 2D cross-section layers of the entire object are created. In the end, the 3D printing process begins with the deposition of the material with the successive sequence of the 2D layers [7, 74].
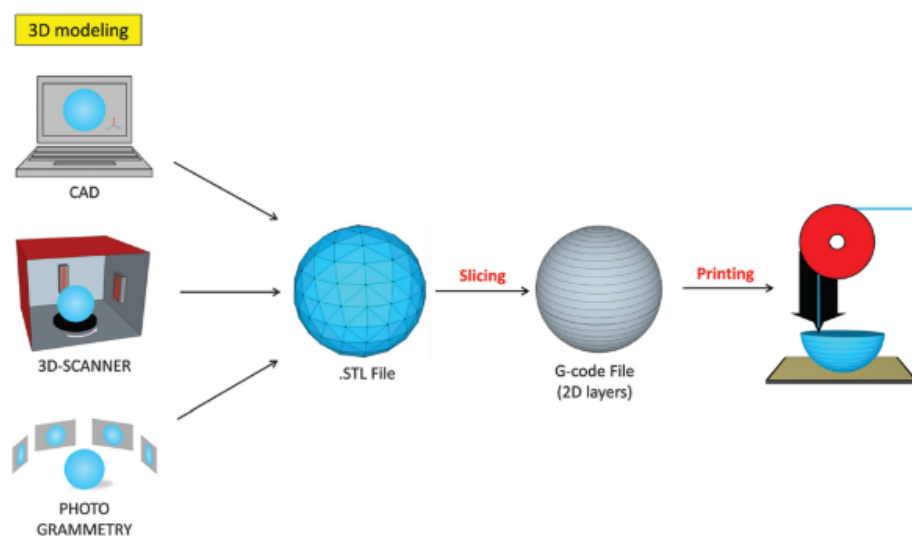
Figure 2.9: 3D-printing process. Obtained from [7].

Several 3D printing technologies have been developed, therefore the ASTM Standard

F2792 classifies this technology into seven groups: binding jetting, directed energy deposition, material extrusion, material jetting, powder bed fusion, sheet lamination and vat photopolymerization [75].

2.5.1   Material Extrusion

The material extrusion is a form of additive manufacturing of polymers with which complex structures are created that other traditional manufacturing techniques could not. In addition, the cost and manufacturing time is reduced with this technique compared to other printing techniques [76]. In the development of this thesis, the materials extrusion technique will be used, where fused deposition modeling (FDM) and Robocasting or Direct Ink Writing (DIW) are sub techniques. The two build the object layer by layer from the bottom (the first layer created on the heated bed) to upwards, heating and extruding filaments. While differentiated by the requirement of additional time to dry or solidify after being deposited, the use of extrusion material will define which sub-technique to use. [77].

Fused Deposition Modeling

The Fused Deposition Modeling consists of the deposition of the material directly through the nozzle head after pretreatment as liquefaction. Therefore, the material is heated to a semi-molten state prior to extrusion through the nozzle. After the material is deposited, it solidifies, creating a uniform hard layer stacked on top of the previous layer depending on the design made. For greater compression, the figure 2.10 shown the parts of the printer for FDM.
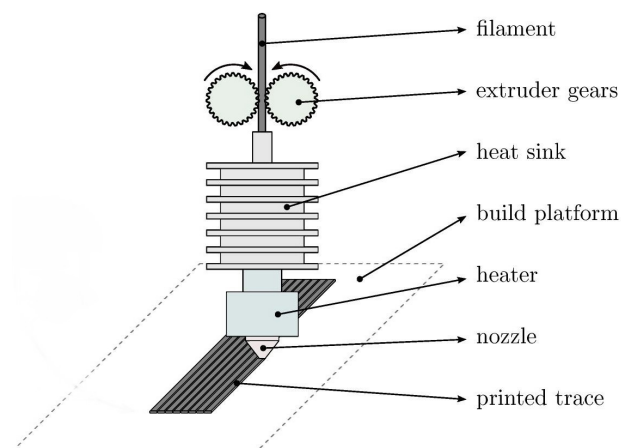
Figure 2.10: 3D printer parts. Modified from [8]

Processing Parameter in Additive Manufacturing

Compression of the 3D printing processing parameters is essential since, otherwise, it is possible that the object with the desired specifications will not be obtained [76]. Some of the parameters for 3D printing are layer height, print heated bed temperature, nozzle temperature and print speed.

- Layer Height: Height of the individual thickness of each layer. It affect the print time and vertical resolution. By choosing taller layer heights you can significantly shorten the print time at the cost of more visible layers. On the other hand, choosing small layer height will result in extra detail at the cost of longer print times [78].

- Material Temperature: Nozzle Temperature and Print Heated Bed Temperature are conditions related to the type of material to be worked on.

- Print Speed: How fast or slow the nozzle moves around to print each layer of the filament. Prints quickly reduce the printing time however, the best quality usually comes from slower printing speeds [79].

- Extrusion Multiplier: Change the amount of flow proportionally. It influence to get nice surface finish and correct single wall widths [78].

2.5.2   Impression Material

The FDM can manufacture objects with a wide range of materials such as elastomers, thermoplastics (acrylonitrile butadiene styrene (ABS), polylactic acid (PLA), polyethylene terephthalate glycolized (PETG), polyvinyl alcohol (PVA), etc), glass, metal and composites [7, 80, 71]. The filament quality is essential since, nowadays, 3D parts can be printed for structural or biomedical applications [81]. Polymers are the most used due to their low cost and hard structural behavior; however, they have a high mechanical and functional resistance [82]. Therefore, several materials have begun to be combined and nowadays composites have been named the materials of the 21st century [83].

Composite

The combination of various materials helps overcome the problems of using a single material, improving durability, thermal and mechanical conditions. Composites can be classified as fiber-reinforced and particle-reinforced. The fiber-reinforced composite polimer matrix helps overcome the limitations of using thermoplastics, which do not have the strength to produce fully functional parts [84, 81]. On the other hand, reinforced particles are easily mixed with polymers, providing flexibility and improving the mechanical and thermal properties in their use with the FDM technique [82, 81]. Some examples are the use of thermoplastic and thermoset matrices such as PLA, ABS, PEG, and polycaprolactone (PCL) filled with Bronze, Carbon Compounds, Copper, etc. have been used [85].There is a wide variety of composites depending on the mixture between matrix and fillex; composites can exhibit various properties, such as electrical or thermal conductivity, self-healing, mechanical load-bearing capacity, and magnetic embedded circuitry necessary for the desired area of application.

2.6   Electrical Characterization

2.6.1   Resistance

The flow of charge through any material finds an opposing force similar to mechanical friction in many ways. This opposition is due to collisions between electrons-electrons and other atoms is called the resistance of the material, which is expressed in ohms (Ω) [86].

To be able to measure the resistance, devices such as the multimeter are used. The multimeter operates on the principle of Ohm's law; therefore, to determine the material's resistance, the meter will create a voltage between the two probes used, inducing a current in the material (Figure 2.11). The provided voltage is constant; the resistance will be proportional to the resulting current [9]. To understand, the corresponding electrical circuit (Figure 2.11) is considered two resistors in parallel where the current will always find the path with less resistance. The thicker the material is, the lower the resistance will be [9].
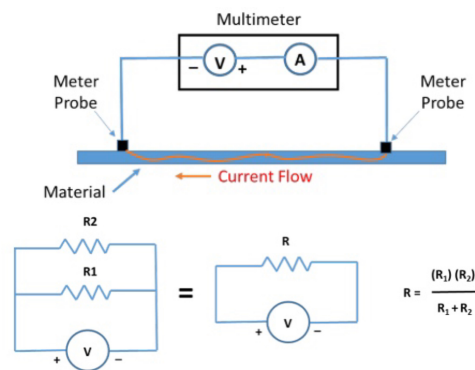
Figure 2.11: Multimeter principle (Up) and corresponding electrical circuit (Down). Modified from [9].

2.6.2   Conductance

Conductance (G) is the reciprocal of resistance (2.1) showing how well a material will conduct electricity; measured in siemens (S).

$$G = \frac{1}{R}$$
$$G = \frac{A}{\rho l} \tag{2.1}$$

2.6.3   Bulk Resistivity

The bulk resistivity ρ is an intrinsic electrical property related to carrier drift in materials [87]. The bulk resistivity could be measured by the voltage drop in a probe through which a direct current flows.

Moreover, the resistivity is described by the formula 2.2:

$$\rho = \frac{RA}{L} \tag{2.2}$$

It describe the normalization of the bulk resistance (R) by its geometrical dimensions due to A= cross-sectional area of the material, and the distance between the two ideal contacts (L).

Pressure Probe

Using the technique of pressure probe, the volume resistivity could be measured; the meter creates a voltage (V) between the top and bottom of the material where a current is induced up and down. The volume resistivity used the formula 2.5.

$$\rho = \frac{RA}{t} \tag{2.3}$$

where:

ρ = Volume Resistivity (Ω-cm)
R = Resistivity (Ω)
A = Surface Area (cm^2)
t = thickness (cm)
The figure 2.12 shows the pressure probe view, showing the current path in red lines. The equivalent circuit for this test is also shown.
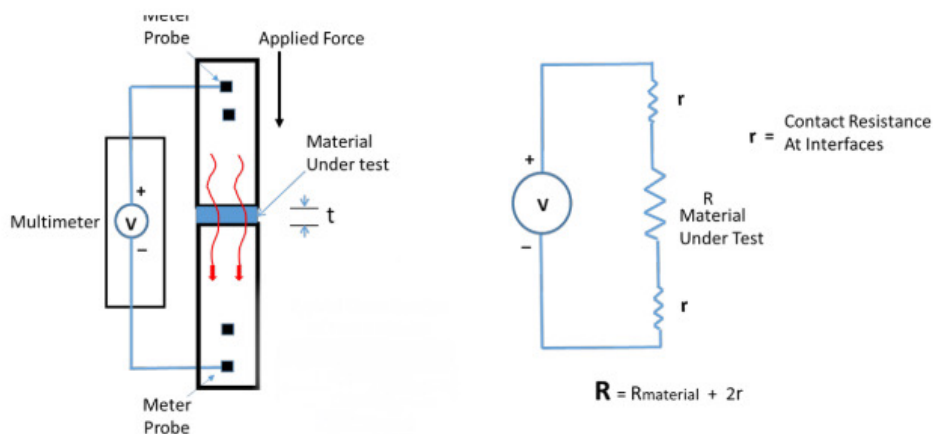
Figure 2.12: Pressure Probe: Blowup view in the left, simplified equivalent circuit in the right. Modified from [9].

Measurement Techniques

To minimize the contribution of contact resistance to the total resistance, techniques such as the two-probe and four-point probe techniques have been developed, which are based on separate current injection and voltage drop measurements. The difference is that the four-point probe solves two-probe problems: lateral contact geometry, probe spacing, and minority carrier injection near the lateral contacts [10]. Two probes are used for the current injection and the other two to measure the voltage drop; as an example, the figure 2.13 shows the configuration of the four-point probe [10]. Probes 1 and 4 are configured for the current, while 2 and 3 handle the voltage; t refers to the thickness of the material and a the initial distance to place the first probe. *S1*, *S2*, and *S3* are called the distance between probes; in the most practical case, these are equal; however, it is not strictly this [10].
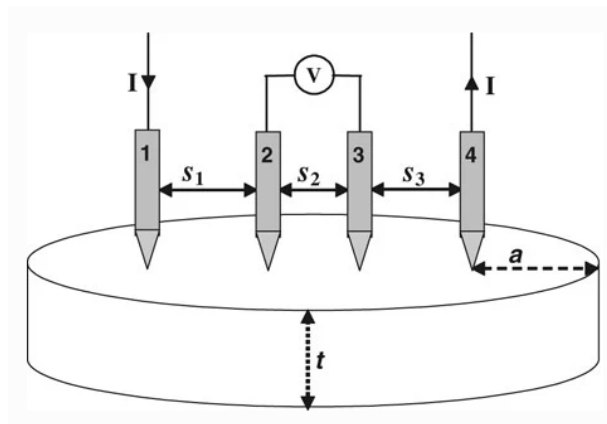
Figure 2.13: Four-point probe configuration. Obtained from [10].

2.6.4   Electrochemical Impedance Spectroscopy (EIS)

Electrochemical Impedance Spectroscopy (EIS) is a technique used for the analysis of interfacial properties related to bio-recognition events occurring at the electrode surface [88].

EIS is a technique used to analyze interfacial properties related to bio-recognition events occurring at the electrode surface. The impedance of the circuit is measured in ohms. The advantages of using this technique are that it is stable, uses small-signal analyses, and works in a vast frequency range (less than 1mHZ to more than 1MHz).

Basic concepts

Impedance differs from resistance because EIS works in DC circuits and is directly based on Ohm's Law. To obtain the impedance response, applying a small driving signal is necessary. A phase shift is acquired from a pseudo-linear response, while the current response to a sinusoidal potential is a sinusoid at the applied frequency.

$$E_t = E_0 * sin(wt) \tag{2.4}$$

where:
Et = potential at time t
E0 = amplittude of the signal
w= radial frequency

From the relationship between radial frequency and the phase shift at different amplitudes in linear systems, the equation defines the impedance of the entire system.

$$Z = \frac{E}{I} = Z_0 exp(i\Phi) = Z_0(cos\Phi + isin\Phi) \tag{2.5}$$

where:
Z= impedance
E= potential
I= current
w=frequency
Φ = phase shift between E and I

Representations of EIS

A Nyquist plot is a current form of EIS representation where the resistive processes are analyzed. The impedance is divided into a real and an imaginary part. Therefore it plots the real part (Zreal) on the X-axis and the imaginary part (Zimag) on the Y-axis, where each point is an impedance value at a frequency point, while Zimag is negative [88].
Another way to plot the impedance results is using the Bode plot, which comprises two separate logarithmic plots like magnitude vs. frequency or phase vs. frequency. This plot is used to evaluate capacitive systems [88].

Chapter 3

State of the Art

This chapter presents an overview of 3D printed dry electrodes with flat surface structure, structure surface, and microneedles on the surface. In addition, the material of the electrodes, 3D printing methods, and electrode dimensions are explained. Likewise, the tests carried out on humans, such as skin impedance and obtaining the cardiac signal.

3.1 Flat Surface Electrodes

Kaveh et al. [11] created electrodes made of methacrylate material, photopolymer with metal, plating of Pd-Tin, and finally catalyzing of Cu and Au, which formed a multi-layer electrode under the method of stereolithography (SLA) 3D printing. The dry electrode has a contact area of 50 mm^2, showing 33 kΩ per cm^2 as electrode resistivity. The magnitude of ESI characterization (0 - 1 MHz) decreases from 100 kΩ to 0.5 kΩ. On the other hand, the time domain measurement of the heart was obtained using a single-lead. In 3.5 seconds of ECG recording, the PQRST complex is observed. Moreover, Chlaihawi et al. [12] used Ag flake ink on a flexible polyethylene terephthalate (PET) to build a dry electrode; a multi-walled carbon nanotube (MWCNT) / polydimethylsiloxane (PDMS) composite was used as conductivity polymer on it. Flat surface electrodes of different sizes (8 mm, 12 mm, and 16 mm radius) were created. EIS was performed at a frequency of 1 – 400 kHz, positioning them on the skin at a distance of 8 cm between the center of each electrode. It shows that the greater the contact area, the lower the impedance obtained; however, it is still a much higher impedance when using wet Ag/AgCl electrodes. The ECG signal, the QRS-complex, P-wave, and T wave are shown, obtaining a 0.95 average correlation between dry and wet electrodes. Finally, a 963.25 $\pm$ 36.82 mV peak to peak amplitude was obtained with the 16 mm radius dry electrode. Moreover, Abdou et al. [13] created electrodes made of proto-pasta conductive PLA. A single lead ECG system was used to identify P, Q, R, S, and T waves and the QRS complex.
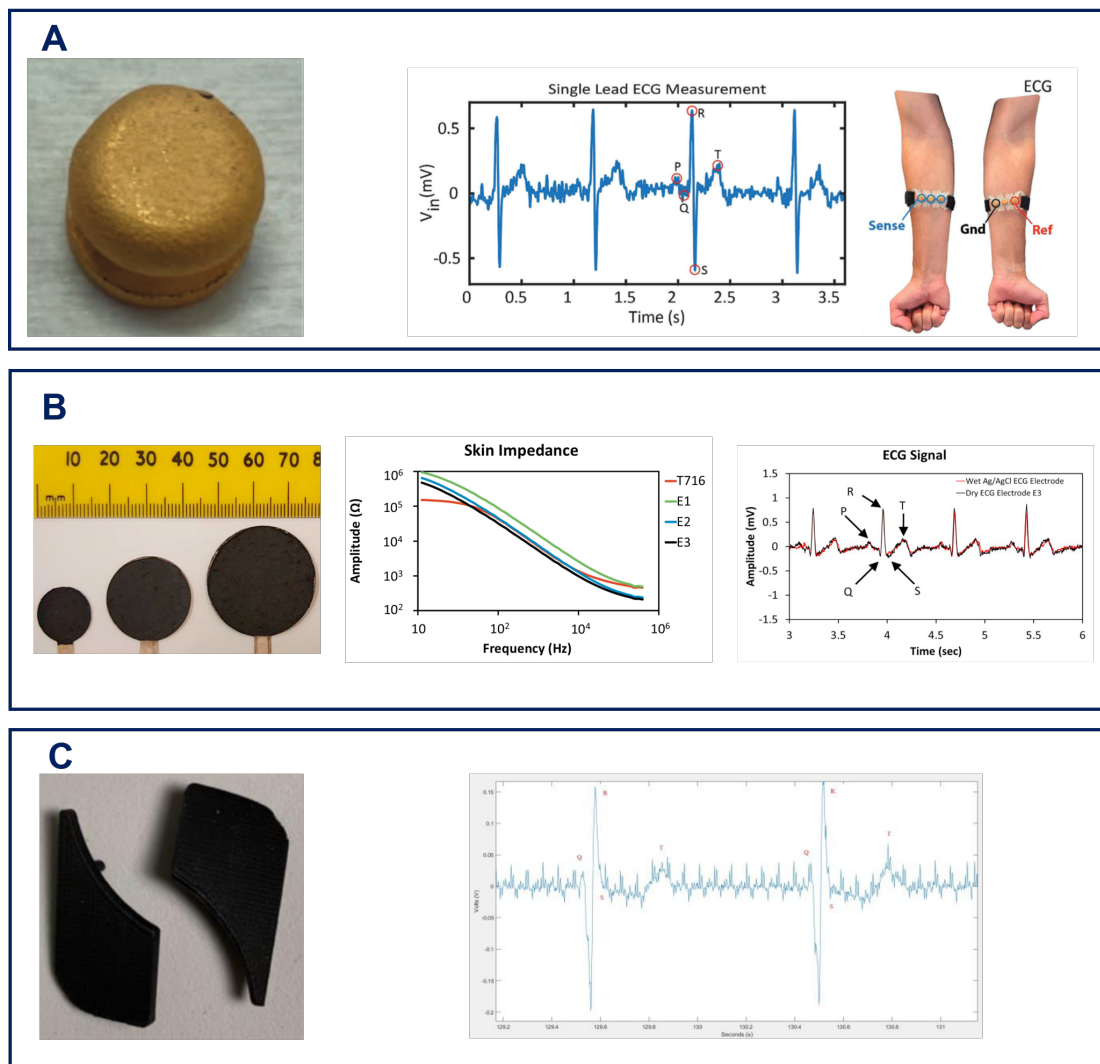
Figure 3.1: Overview of 3D printed flat dry ECG electrodes. A) dry electrodes obtained ECG signal, PQRT complex is observed [11]. B) MWCNT/PDMS dry electrodes of different sizes (8 mm, 12 mm, 16 mm) [12]. C) Proto-conductive paste PLA electrodes obtained the cardiac signal, displaying the P, Q, R, S, and T waves and the QRS complex [13].

3.2   Structure Surface Electrodes

Dos Santos Silva et al. [14] created a home ECG monitoring with PolyLactic Acid (PLA) electrodes printed under FDM. The electrodes presented a superficial pyramidal texture placed in a toweled seat. The lowest resistance (30 Ω per cm on the Y-axis and 115 Ω per cm along Z-axis) was obtained at a higher printing temperature (230<) than specified by the filament distributor. The results show a good waveform morphology with 0% signal loss and an above 0.99 Pearson correlation coefficient (r) with wet commercial electrodes. The Heart Rate shows a difference of -1.78 $\pm$ 4.65 between the HR of the elaborated electrodes (76.62 $\pm$ 8.48) and the reference (78.39 $\pm$ 8.45). Besides, Meng et al. [15] created a

flexible array with microdomes PDMS-based (Polydimethylsiloxane) electrodes where its fabrication was composed of melting photoresist, double-PDMS-molding, Ni plating, and finally, an encapsulation between two PDMS films. The skin-electrode contact impedance was compared between 40x40, 60x60, and 80x80 arrays, where the impedance was slightly higher for the 80x80 array than for the commercial electrodes. It is observed that the impedance decreases as the contact area increases. The dry electrode stability was shown where the impedance is similar to the commercial electrode at the beginning. However, over time the impedance of the Ag/AgCl electrodes increased dramatically after one hour. This is due to the dehydration of the gel used in commercial electrodes, which deteriorates over time. On the other hand, using the 3-lead ECG, it is observed that the larger array size shows less noise due to more contact with the skin. The cardiac signal obtained with the 80x80 array is similar to the Ag/AgCl electrodes. Moreover, using the FDM 3D Printing technique, Kim et al. [16] created a NinjaFlex material plus conductive silver paste leech-inspired origami (LIO) dry electrodes. The signal obtained does not show a significant difference between the wet and origami dry electrodes and, the peaks are also highly distinguishable. The signal to noise ratio shows a value of 21.7 $\pm$ 0.56 dB for LIO sensor while a value of 18.1 $\pm$ 0.85 dB for wet electrodes. Additionally, cardiac measurement was performed while performing exercises such as climbing 100 and 200 stairs and after exercising.
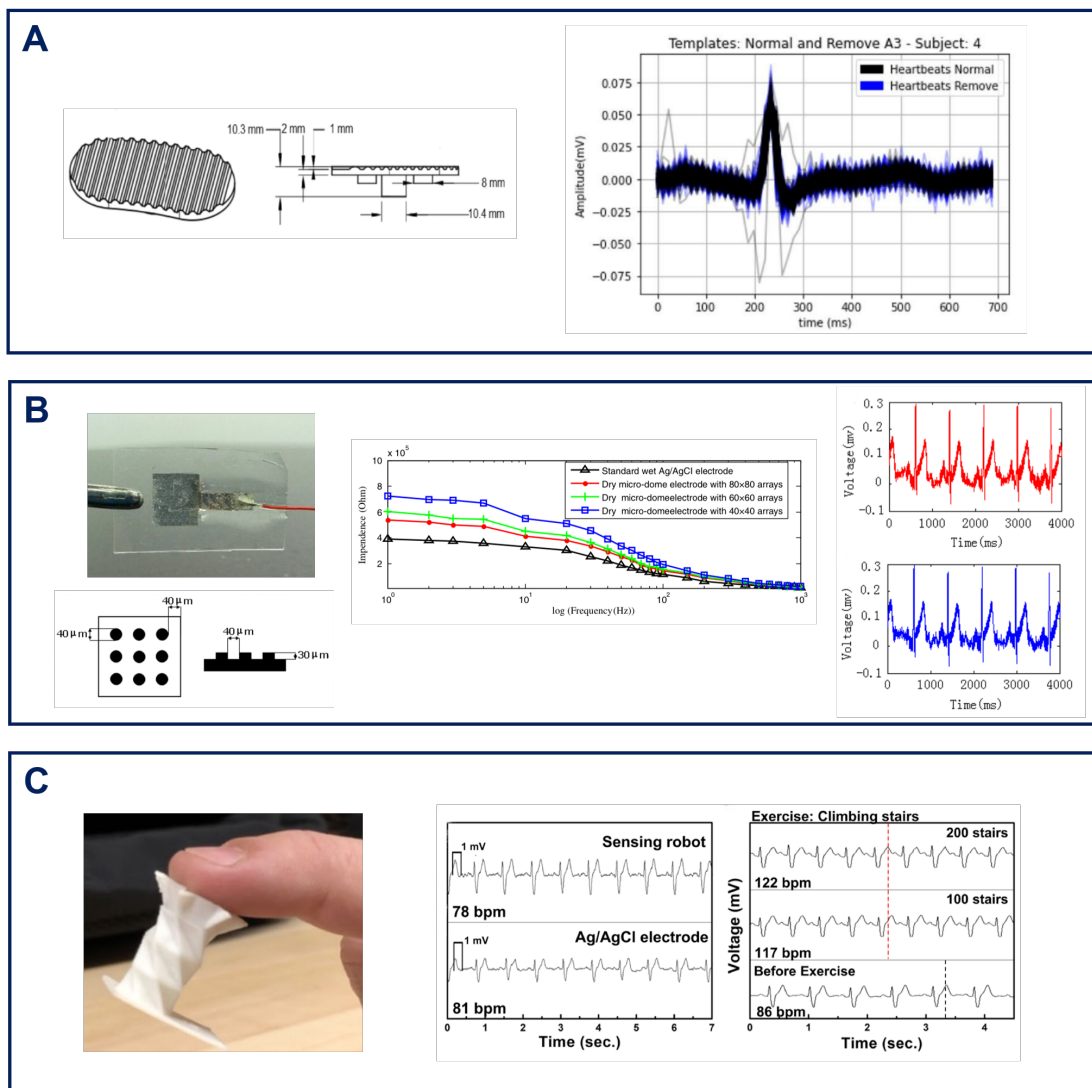
Figure 3.2: Overview of dry ECG electrodes with 3D printed structure surface. A) PLA electrodes with superficial pyramidal texture obtained the cardiac signal [14]. B) flexible 80x80 array with microdomes PDMS-based electrodes, which obtained a slightly higher skin impedance than with commercial electrodes, as well as a similar morphology in the cardiac signal [15]. C) IOL dry electrodes obtained cardiac measurement during climbing 100 and 200 stairs and after exercise [16]

3.3   Microneedle Surface Electrodes

Salvo et al. [17] created 3D printing dry electrodes, which consist of 180 conical needles (3 mm high) of a polymeric material placed on the surface with a distance of 250 μm between them, intending to have a large contact area and not be sharp enough that pierce the skin. The electrode-skin impedance was measured on the chest at a frequency of 0-0.8 kHz, obtaining a magnitude of around 190-90 kΩ. On the other hand, a 3-Lead ECG

was performed, which recorded the cardiac signal where two similar signals were obtained between wet and dry electrodes.
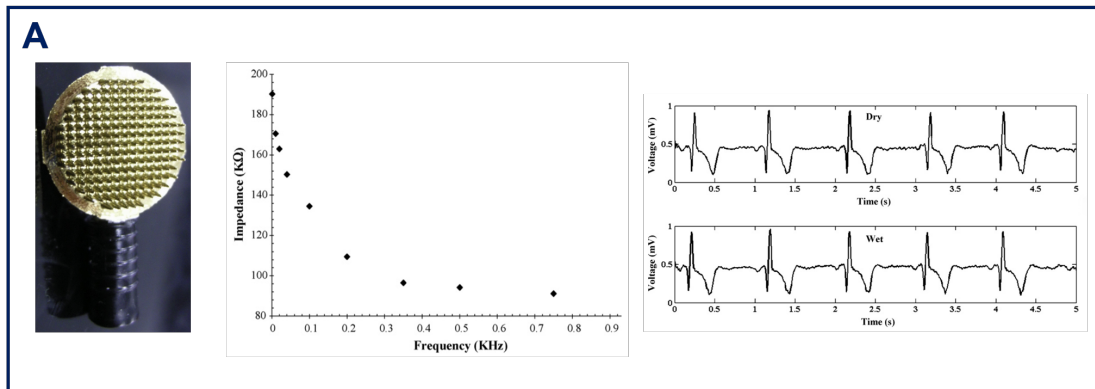
Figure 3.3: 3D printing dry electrodes with 180 conical needles on the surface were used to measure the chest skin's impedance and obtain a similar cardiac signal between wet and dry electrodes [17].

Table 3.1: Summary of the state of art of 3D printed electrodes for ECG

Manufactory Method	Material	Morphology	Resistivity /Conductivity	Skin-electrode Impedance	Cardiac Signal Acquisition Data	Ref
SLA 3D Printing	Methacrylate photopolymer Plating of Pd-Tin Catalyst, Cu and Au	Flat surface	33 kΩ cm^2	0 -1 MHz 100 – 0.5 kΩ	PQRST complex observation	[11]
FDM 3D Printing	PLA	Pyramidal surface	30 Ωcm in Y axis 115 Ωcm in Z axis	-	0% signal loss r = 0.99 ΔHR = -1.78 $\pm$ 4.65	[14]
Molding (FDM 3D Printing)	Melting Photoresist Ni plating Encapsulation between PDMS films	80x80 array microdomes at the surface	-	2V 10 – 10 kHz (500 - 100) kΩ	Morphology similarity	[15]
FDM 3D Printing	NinjaFlex Conductive Silver Paste	LIO	-	-	SNR = 21.7 $\pm$ 0.56 dB Peaks Highly Distinguishable	[16]
Inkjet Printing	Ag flake ink PET substrate MWCNT/ PDMS composite	8mm radius Flat Surface	938.8 mS cm (at 8% weight ratio of MWCNT/PDMS)	1 – 400 Hz ($10^6 – 10^2$ Ω) 524 kΩ (At 1 Hz)	0.95 average correlation 963.25 $\pm$ 36.82 mV (at peak to peak amplitude)	[12]
PolyJet Printing	Polymeric material	Microneedle 180 conical needles	-	0 - 0.8 kHz 190 - 90 kΩ	Similarity of signals	[17]
FDM 3D Printing	Conductive PLA	Flat electrode	-	-	P, Q, R, S, T wave QRS complex observation	[13]

Chapter 4

Materials and Methodology

This chapter describes the materials used to print the electrodes and the devices used for material and electrical characterization, such as the creation of the system to acquire the cardiac signal. Additionally, it explains the methodology followed to meet the objectives set out in the thesis.

4.1 Materials

4.1.1 Chemical and Materials

Electrifi by MULTI3D, a biodegradable polyester and cooper conductive filament with 0.006 Ω/cm, was used to print the dry electrode [36]. The Colloidal Silver Liquid from Electron Microscopy Sciences was used to improve the electrical contact of the printed surface of the electrodes [89]. For the electronic characterization experiments regarding the adhesion of the dry electrodes to the skin, 48 mm wide masking tape and 50 mm wide micropore medical tape of the 3M brand were used. An Olympian brand wrist strap was used to apply pressure to the electrodes. For the electrode adhesion experiment with the body cream, Neutrogena Hydro Boost was used because its consistency is light and compatible with all skin types, even sensitive. Hence, the 6 cm diameter 3M Red Dot cloth adult EKG/ECG commercial electrode is used as a comparative Ag/AgCl hydrogel electrode with dry electrodes [90]. For the development of the cardiac signal acquisition system, two AD8232 ECG modules, two Arduino UNO, and an ASUS TUF DASH F15 computer were used, in addition to male-to-male cables to connect the Arduino and the modules and USB cables for the Arduino-Computer connection.

4.1.2 Devices

The dry electrode was 3D printed under the Hydra 16A S Standard 3D printer from the Hyrel International, Inc (HYREL 3D) [91]. For the characterization of the material and to obtain more detailed images and micro and nanometric scale, the Nikon SMZ 1500 Stereomicroscope and the FEI Phenom Personal Scanning Electron Microscope (SEM)

were used. Additionally, a Bruker brand profilometer is used to obtain the profiler of the contact surfaces of the dry electrodes.

To obtain the resistance measurements, both a parameter analyzer device and a commercial digital multimeter were used. Keithley's Parameter Analyzer is a customizable and fully-integrated parameter analyzer that provides synchronized insight into current-voltage (I-V), capacitance-voltage (C-V), and ultra-fast pulsed I-V characterization, accelerating semi-conductor,materials, and process development [92]. A SemiProbe high-frequency machine is connected to the Keithley device. The SemiProbe machine uses components such as needle-optimized manipulators to work precisely and with tiny and detailed semiconductor designs [93]. The digital multimeter used is the CD800a by SANWA which measures low-voltage circuit [94]. For the impedance measurement, the Impedance Analyzer, PalmSens4 was used. It has a large potential range from -10 V to 10 V and a current range from 100 ρA to 10 mA with a high resolution and low noise [95].

4.2   Methodology

4.2.1   Fabrication of Dry Flexible Electrodes

The manufacturing process of flexible dry electrodes encompasses the design, and the 3D printing conditions and settings.

Design

The digital models of the 3D flexible electrode were designed in the SolidWorks environment. The design consists of a cylinder where the shape (Diameter: 7 mm, 15 mm, 23 mm, 30 mm; Thickness: 0.3 mm) will be studied. To maintain the flexibility of the electrode, the thickness was kept at 0.3 mm, that is, a single printing layer to present more flexibility due to the bulky design. After that, an STL format file for each combination was made. Then the PrusaSlicer Software was used to convert the STL file data into a G-code file. Finally, the printer used this information to 3D print the dry electrodes.

3D Printing

The additive manufacturing 3D process printing begins with the choice of material. For the experiment, the Electrifi filament was deposited in a horizontal layer-by-layer fashion on a flat smooth surface like a bed/platform of the Hydra 16A 3D printer. Also, the 3D printing used a 0.5 mm nozzle size. Likewise, printing settings like print Speed: 5 mm/s, Fan Speed: 50%, Fill density: 100% and Infill Patter: Concentric were selected for all the printing with the Electrifi filament. However, printing settings like Heated Bed and Nozzle Temperature for the filament mentioned above are studied in this thesis for its influence on electrical characterization.

Placement of Colloidal Silver Liquid

For the resistance measurements of each electrode in the temperature variation experiment, the colloidal silver liquid is placed in the center of the top and bottom surfaces of the electrode. It is also placed on the upper surface in the opposite outer ones aligned in a straight line through the middle of the circumference of the electrode.

For impedance measurements, the colloidal silver liquid is placed in the center of the electrode and acts as a glue between the non-contact surface with the skin and the previously cut 5 cm wire.

4.2.2   Printing setting: Temperature and its relation with the resistance measurements

To experiment with the temperature of the heated bed (40°, 110°) and nozzle (140°, 150°, 160°), an electrode of Diameter: 15 mm and Thickness: 0.3 mm was printing. The table 4.1 shows the label of all the combinations of heated bed (b) and nozzle (n) as printing settings for each trial. Six temperature combinations are obtained for which the resistance test measure for each one.

Table 4.1: Label of printing settings combinations for Temperature trials.

b40t140	b40t150	b40t160
b110t140	b110t150	b110t160

Resistance

The resistance of the individually printed electrodes is measured to determine their current flow conductance capacity and their potential to be used for bioimpedance measurements. Additionally, the temperature and the drying time of the silver paste to improve the electrical conductivity are important parameters that will help obtain the electrode with the best conductance. Therefore, two resistance measurements (Top-Bottom, Edges) of each printed electrode were developed with two different devices (Multimeter and Parameter Analyzer (Keithley)).

To measure the resistance between the electrode's edges with the multimeter, place the electrode on an insulating surface and place each tip of the multimeter on each side where the colloidal silver liquid was placed on the non-contact surface. The measurement was made after 6 hours of colloidal silver liquid drying. After the multimeter measure, the Keithley+Semiprobe device was used to obtain a more precise resistance value. The needles of the Semiprobe machine were operated using the 4-point-probe technique. Two needles are placed on each side (right, left) of the colloidal silver liquid of the electrode. The setups for the measurements with the two devices are shown in Figure 4.1.
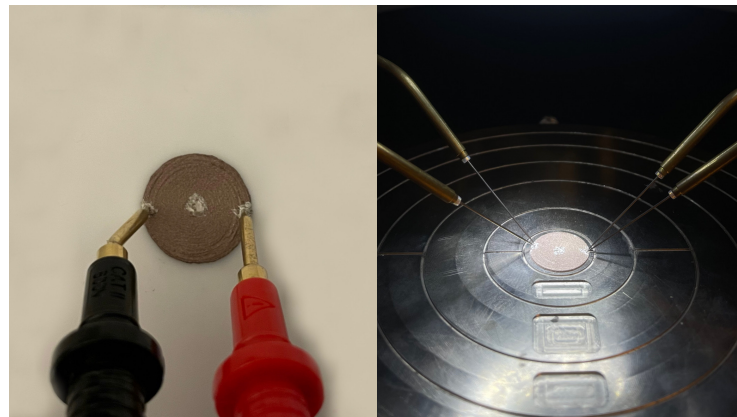
Figure 4.1: Measurement of the resistance between the edges of the electrode with the multimiter (left) and the Keithley+Semiprobe device (right).

To measure the top and bottom surface resistivity of the electrode with the multimeter, a holder based on four movable arms with crocodile heads was used to hold two plates of clear acrylic sheets previously modified for use in electrode measurements. The clear acrylic sheet is placed, then the dry electrode and finally another clear acrylic sheet, one on top of the other in that order so that the same pressure is applied to each part of the electrode. Also, the sheets helps avoid contact directly between the electrodes and the crocodile clips to avoiding any deformation. To measure the resistance with the Keithley+Semiprobe device, the same setup with the clear acrylic sheets mentioned above was used. However, a weight is applied to each side of the sheets for this setup to keep the wires pressed and stable to the electrode surfaces. Alligator-tipped wires are used to connect to the needles of the semiprobe machine and use the 4-point-probe technique. The setups for the measurements with the two devices are shown in Figure 4.2.
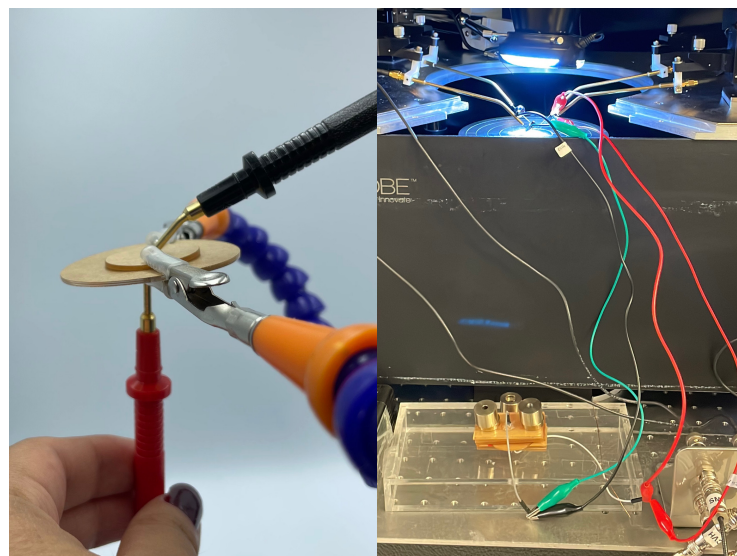
Figure 4.2: Measurement of the resistance between the top and bottom surfaces of the electrode with the multimiter (left) and the Keithley+Semiprobe device (right).

Resistance over time

The objective is to see the relationship of the drying time with the resistance obtained in the electrodes. The colloidal silver liquid is placed, and, as recommended by the manufacturer, it is allowed to dry at room temperature. Resistance is measured in the manner mentioned in the previous section after 16 hours (estimated drying time by the company) and then at 19, 24, 36, 48, 60, 72, 84, 96 hours after laying.

4.2.3 Diameter and Texture: Its relation with the Electrical Characterization

Electrode Characteristics

The printing settings of the electrode in this section were based on the resistance results from section 4.2.2, which are described in the results section. Therefore, two different combinations (b40t140, b110t140) are used to compare in the electrical characterization section.

For this section, electrodes with different diameters (7mm, 15mm, 23mm, 30mm) with a thickness of 0.3 mm were designed. The chosen dimensions were based on state of the art found, and also it was considered that they must have dimensions that maintain the ability to be bent and twisted. This criterion was used by Wang et al. [96] to define dry electrodes as flexible.

Each electrode was printed with the two temperatures mentioned previously. However, two sets of electrodes are printed because the contact surface structure is a factor to study in the electrical characterization section. Two different surfaces are obtained when printing: (smooth, concentric). Smooth refers to the surface in contact with the aluminum heated bed from the 3D printer, which has a very smooth finish. Concentric is the infill pattern used in printing, and this structure is visible on the upper surface of the electrode. The table 4.2 is presented for a better understanding of the parameters and dimensions used, it shows the 16 pairs of electrodes printed.

Table 4.2: Surface texture, temperature settings and dimensions of the printed electrodes for the electrical characterization.

Surface Texture	Concentric		Smooth	
Temperature Settings	b40t140	b110t140	b40t140	b110t140
Dimensions (diameter x thickness)	7x0.3 (mm)	7x0.3 (mm)	7x0.3 (mm)	7x0.3 (mm)
	15x0.3 (mm)	15x0.3 (mm)	15x0.3 (mm)	15x0.3 (mm)
	23x0.3 (mm)	23x0.3 (mm)	23x0.3 (mm)	23x0.3 (mm)
	30x0.3 (mm)	30x0.3 (mm)	30x0.3 (mm)	30x0.3 (mm)

4.3   Material Characterization

4.3.1   Stereomicroscope

The Nikon SMZ 1500 Stereomicroscope was used to capture more detailed images of the electrode and define more noticeable differences between the surfaces in contact with the skin, which are analyzed in the electrical characterization section.

4.3.2   SEM spectroscopy

The characterization of the electrodes with SEM spectroscopy was carried out to distinguish the differences of the structures of the surfaces in contact with the skin and how they change with respect to the applied temperature during 3D printing.

4.3.3   Profilometer

The profilometer is used to measure the profile of the electrode contact surfaces to quantify their roughness related to the printing temperature of the electrodes.

4.4   Electrical Characterization

4.4.1   EIS Settings

For EIS, an AC signal of a set amplitude range from 10 μV to 10 mV is applied in a sinusoidal wave form for a frequency range of 0.1 Hz to 300 kHz on top of the DC offset.

4.4.2   Frequency Response of Electrodes

EIS was performed from two electrodes of the same diameter aligned to each other. For that, the setup shown in the Figure was used where two large binder clips, one on each side of the aligned electrodes, were colocated to maintain good contact between their surfaces. The black plastic of the large blinder clips is a material that does not conduct electricity [97] and therefore does not affect the EIS measurements. The crocodile leads of the PalmSense4 were matched to the wires previously attached to the printed electrodes as shown in figure 4.3.
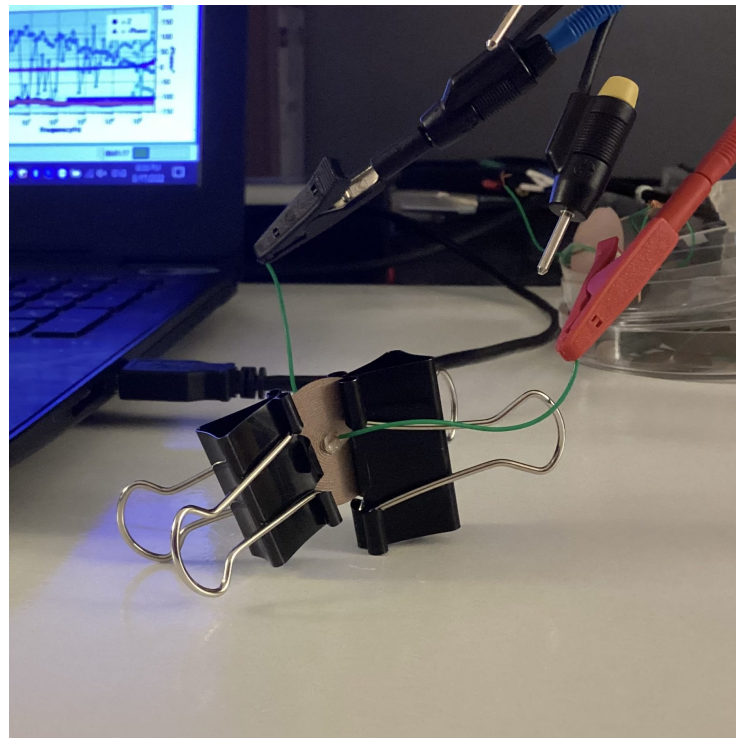
Figure 4.3: Setup for the frequency response of the electrodes

4.4.3   Skin Impedance

Experimental Setup and Preparation of skin

Several steps are performed to prepare the setup to measure the impedance between the created electrodes and the human skin.

1. Two printed electrodes with the exact diameter and printing conditions are used.

2. Strip two wires from one side, and use the silver paste to attach the stripped side to the top of the electrode and let it dry at room temperature for two days. The time for letting the silver colloidal liquid dry was concluded after the Temperature influence on the resistance measurement section.

For the measurement of the impedance of the electrodes in the skin, there is a process to follow to prepare the skin and the position of the electrodes there.

- The arm was washed with soup and water around a hour before the experiment.

- The first electrode was place five centimeters from the wrist, and the second one 5 cm from the first one. The electrode must be place at 5 cm from center to center between electrodes.

Overtime Stability

The effect of the dependence of the electrodes on the positioning time on the skin will be studied to continue with the other points to study described in this methodology. The other measurements will be made from the time of the result where the impedance measurements stabilize at the frequency of 100 kHz. It is measured for a time of 30 minutes with measurements every 0.1 s. The selected electrodes are the "b110t40" and are adhered to the person's forearm with the Micropore medical tape.

Adhesion of the dry electrodes

Various forms of adherence of the electrodes to the skin are carried out to measure the EIS, such as:

1. The electrodes were placed and fully covered with a Micropore medical tape; a hole was made to let the electrode's wire not be covered by the micropore and be easy to connect with the crocodile wires from the PalmSense4 device.

2. In addition to the dry electrodes used above to compare their adherence, a pair of Ag/AgCl hydrogel electrodes as a commercial comparison was used.

The Figure 4.4 shows the four different adhesion setups of the dry flexible electrodes with the skin.
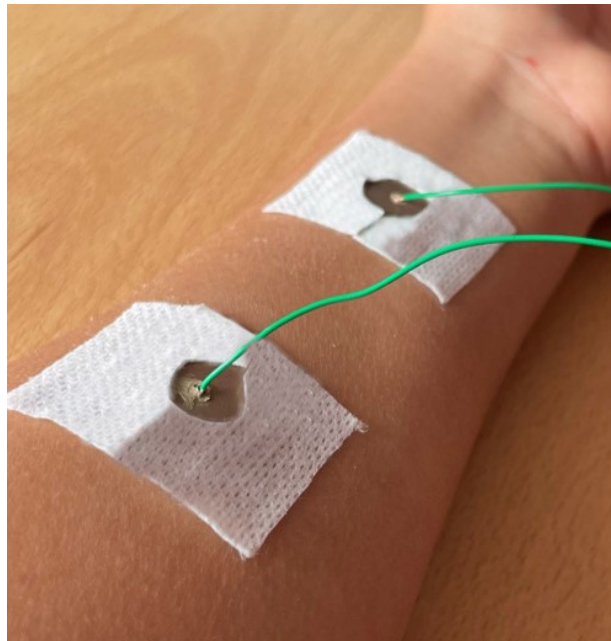
Figure 4.4: Micropore medical tape for adherence of the contact surface of the electrodes with the skin.

Applied force and its relationship with skin impedance measurements

It is studied if there is a dependency between the force applied to the electrode and the measurements of impedance with the skin, for this the electrodes were placed with masking

tape to ensure the electrode's location; a wrist strap on top of the two electrodes was used and kept the other side of the wire exposed to connect with crocodile wires from the PalmSense4 device.Three levels of force are applied (normal, medium, hard), with normal being the force applied only by the wrist band, medium applying a little additional pressure, and hard adjusting it tight enough but being careful not to cut off the circulation of the forearm or cause extreme discomfort to the person.

.,

Figure 4.5: Wrist strap to apply force over the dry electrodes

Skin preparation

The use of body lotion as an adhesion aid for dry electrodes was studied. A body cream was placed on the forearm, leaving a thin layer. The electrodes were placed in the previously stipulated marks, and the cables were connected to the crocodile wires of the PalmSense4 device.

4.5   Electrocardiogram Measurements

The performance of the dry electrodes fabricated in this thesis is investigated by monitoring the ECG signals and comparing them with the signal obtained with the wet Ag/AgCl electrodes.The methodology for obtaining the cardiac signal is separated into three subsections; Hardware, Software, and Setup.The ECG measurements were made simultaneously on the subject, comparing the two types of electrodes.

4.5.1   Hardware

The electronical created system is based on the configuration between the two AD8232 module, an two Arduino UNO coneccted both to an ASUS TUF DASH F15 Computer 4.6. The AD8232 ECG Module is made up of Analog Devices' AD8232 IC which is a chip

designed to extract, amplify and filter biopotential signals to obtain ECGs for example, which are usually extremely noisy signals [18]. Thus, the AD8232 single-wire heart rate monitor acts as an operational amplifier to clearly obtain the PR and QT interval of the cardiac signal [18]. The module, fully integrated single-lead ECG front end, it has a common-mode rejection ratio: 80 dB and DC to 60Hz and it could work with the two or three electrode configurations. The microcontroller board based on the ATmega328P is named Arduino Uno. It has 14 digital input/output pins where 16 MHz ceramic resonator, a USB connection, a power jack, an ICSP header and a reset buttom [19]. Finally, the ASUS TUF DASH F15 laptop was used, which has an 11th Gen Intel CORE 17-11375H CPU, NVIDIA GeForce RTXTM 2070 GPU, and 32GB of DDR4-3200 [20].
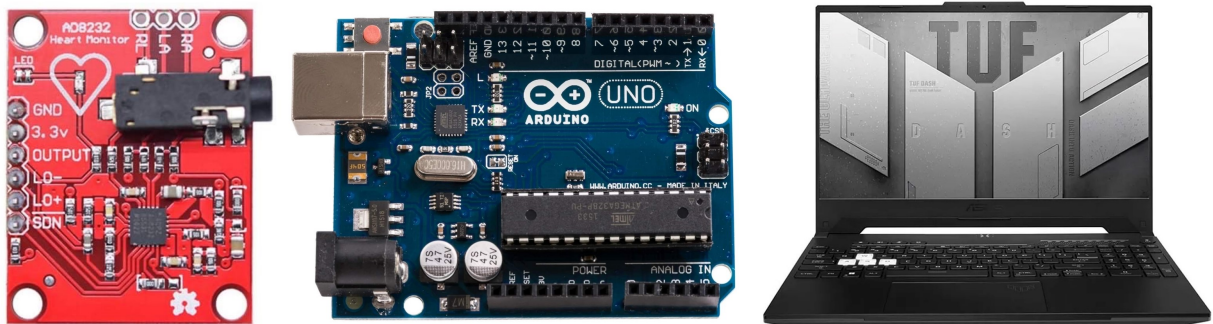
Figure 4.6: From right to left, ECG module [18], Arduino UNO [19] and ASUS Computer [20]

Configuration

To make the connections between the Arduino Uno and the AD8232 ECG module, the following table explains the pin description of each one to create the connection ECG Module-Arduino; additionally, it is presented in a better way in the circuit diagram. These connections work for the two ECG Module-Arduino, one for dry electrodes and the other one for commercial Ag/AgCl electrodes.

Table 4.3: PIN Connections of Arduino UNO

Board Label	Pin Function	Arduino Connection
GND	Ground	GND
3.3v	3.3v Power Supply	3.3v
OUTPUT	Output Signal	A0
LO-	Leads-off Detect -	11
LO+	Leads-off Detect +	10
SDN	Shutdown	Not used

Table 4.4: Pin description of the AD8232 ECG Module

Pin Name	Description
GND	Power Supply Ground
3.3 v	Power Supply 3.3v
OUTPUT (ADC)	Operational Amplifier Output. The fully conditioned heart rate signal is present at this output.
LO-	Leads Off Comparator Output. In DC leads off detection modem, its low when the electrode is connected and high when the electrode to -IN is disconnected.
LO+	Leads Off Comparator Output. In DC leads off detection mode, LOD+ is low when the +IN electrode is connected and high when is disconnected.
SDN	Shutdown Control Input. Drive SDN low to enter the low power shutdown mode.
RA (Right Arm)	RED Biomedical electrode pad RA. Instrumentation Amplifier Negative Input. -IN is typically connected to the right arm (RA) electrode
LA (Left Arm)	YELLOW Biomedical electrode pad LA. Instrumentation Amplifier Positive Input. +IN is typically connected to the left arm (LA) electrode.
RL (Right Leg)	GREEN Biomedical electrode pad RL. Right Leg Drive Output. Connect the
3.5mm ECG Biomedical Electrode Connector Jack	Combine Biomedical Electrode pad Connector of RA,LA and RL.
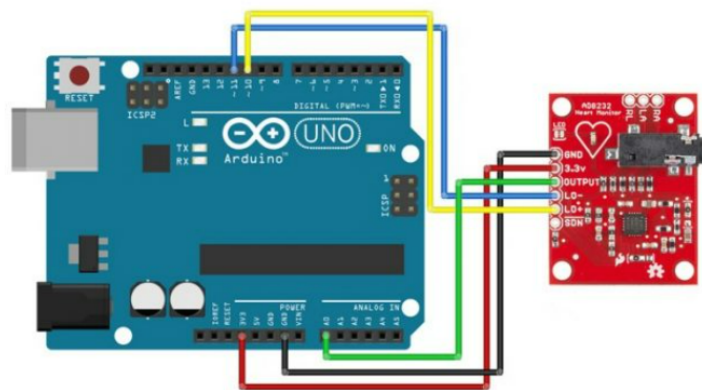
Figure 4.7: ECG module connection with the Arduino UNO

4.5.2   Software

The Laboratory Virtual Instrument Engineering Workbench (LabVIEW) 2020 software from National Instruments is used, a graphical programming environment to develop automated research, validation, and production test systems, in this case, for the acquisition of the cardiac signal [98]. LabView helps us to perform the parallel reading of two Arduino UNO that, in turn, receive the data from the two AD8232 ECG modules; the first uses the electrodes developed in this thesis, while the second uses commercial electrodes.The data is saved in a csv file.

4.5.3   Cardiac System Setup

The 3-wire ECG lead placement was used to record the cardiac signal. According to Wang et al. [99], who did a study of the placement of the electrodes in the chest with the 3-lead configuration, the following diagram 4.8 is selected to be used for the ECG recording in this thesis.RA, LA, and LL are the three electrodes that will be used to connect to the cables supplied with the ECG module. The table shows the connections.
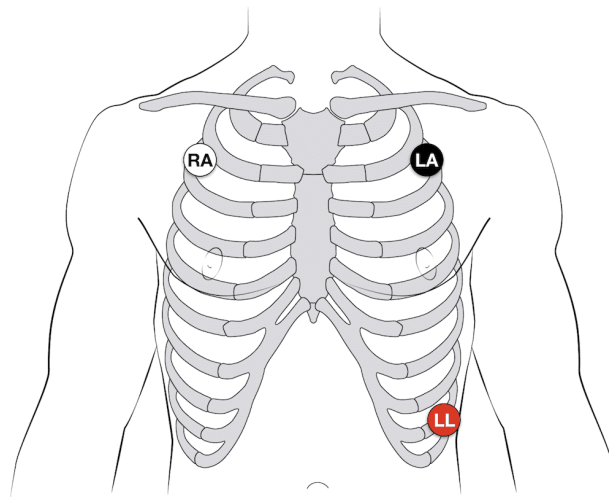
Figure 4.8: Placement of the three electrodes. Obtained from [21].

Table 4.5: Electrode-wire connection

Electrode Name	Wire Color	Location
RA	Red	Right Shoulders-Chest
LA	Yellow	Left Shoulders-Chest
RL	Green	Left Lower Abdomen

Additionally, the test subject is placed in a chair where they feel comfortable, relaxed, and completely calm. To compare simultaneously the two types of electrodes, it was essential to control and have the most similar conditions; one electrode of each type was placed in the position of RA, LA, and LL. In addition, the only previous preparation on the skin was for the subject to wash his chest with water and dry it, so that the corresponding measurements could be carried out after an hour.

4.6   Effect of electrodes on the skin

This section shows whether any skin effects occurred during the experiments.

Chapter 5

Results

This chapter summarizes all the findings for each section of the methodology: 3D printing, the selection of parameters to optimize the conductivity of the electrodes, and the electrical and material characterization. The results obtained are based on the resistance, conductivity, resistivity, and frequency response of the electrodes' impedance and contact with the skin. Finally, the cardiac measurements are present.

5.1 Temperature and its relation with the resistance measurements

The printing settings, such as the heated bed and nozzle temperature, were studied. The figure 5.1 shows the printed electrodes with their respective labels.

Figure 5.1: Electrodes printed with diferent temperatures of the bed and nozzle.

For each of the electrodes shown in figure 5.1, the measurements of the edges of the electrode made with the multimeter and the average of the resistance measured with the Keithley + Semiprobe device over time are shown.

Label	Device	Resistance (Ω) measurements over time (h)								
		16	19	24	36	48	60	72	84	96
b40t140	M	22	23.6	21.8	21.5	20.2	19.5	18.7	17.4	17.4
	K	21.344	23.214	21.238	21.457	19.627	19.135	18.496	17.226	17.267
b40t150	M	182	135	64	63.3	63	61	60	46.6	46.4
	K	181.356	134.400	63.414	63.368	62.521	60.676	59.778	46.406	46.207
b40t160	M	200	206.8	177.4	170.3	155	163.4	157.1	160.3	154
	K	199.323	206.263	176.872	170.326	154.536	163.073	156.804	160.135	153.863
b110t140	M	13.1	12.6	12	11.8	11.5	10.9	10.7	9.4	9.4
	K	12.485	12.973	11.404	11.857	11.836	10.593	10.400	9.283	9.280
b110t150	M	35	29.4	28.3	28.1	27.9	26.1	24.6	22.9	22.9
	K	34.325	28.883	27.700	28.146	27.467	25.736	24.309	22.727	22.737
b110t160	M	820	704	690	658	641	580	554	503	470
	K	819.344	703.456	689.408	658.735	640.566	579.66	553.706	502.847	469.857

Table 5.1: Measurement of resistance between the edges of the electrode over time. (M) Measurements did with a multimeter, (K) Measurements did with a Keithley + Semiprobe device.

From this table, the drying time of the colloidal silver liquid is defined to obtain stable results; after four days of drying, the measurements of the following points begin to be made. The table shows that the electrode labels (b40t160 and b110t160) are not stable between 84 and 96 hours of drying. It may be because the printing temperature of the nozzle is the highest limit recommended by the factory to work with Electrifi, damaging its components. Likewise, in the b110t160, it helps the influence of the high temperature of the heated bed modifies the material's behavior. The other electrode labels are stable since 84 of drying. Moreover, the figure 5.2 shows the resistance obtained over time for all samples (left) and focuses on the three samples with the lowest resistance values (right), in this case, b110t140, b110t150, and b40t140, which are clearly stable since 84 hours of drying.
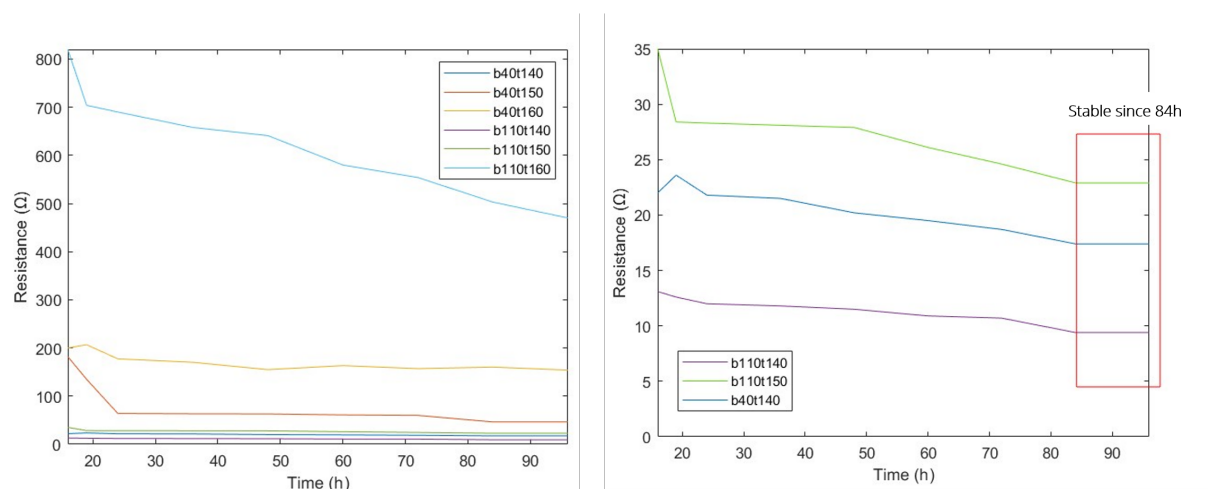
Figure 5.2: The effect of dry silver liquid on resistance.

The following table shows the resistance values taken after 94 hours of drying of the colloidal silver liquid. Measurements are from top to bottom and on the edges of a single electrode. Since the human presence influences the resistance measurements with the multimeter, only the measurements made with the Keithley + Semiprobe device will be shown.

Average Resistance (Ω)		
Label	**Edges**	**Top to Bottom**
b40t140	17.267	187.357 K
b40t150	46.207	17.560 M
b40t160	153.863	90.846 M
b110t140	9.280	4.303 K
b110t150	22.737	602.749 K
b110t160	469.857	170.473 M

Table 5.2: Measurement of the edges and top to bottom of a single electrode

The table 5.2 shows that the labels (b40t140, b110t140, b110t150) are the electrodes with the lowest resistance both between edges and top to bottom. Despite having resistance between top to bottom in kΩ, which is high, they remain much lower than the measurements in the other electrodes with MΩ.

The figure 5.3 are the three best electrode labels' graphs of resistivity, conductivity, and resistance. To calculate the volumetric resistivity measuring under a pressure probe, the surface area is 7.0686 cm^2, and the thickness is 0.03 cm. For the volumetric resistivity of a surface probe, the cross-sectional area of the material is 0.045 cm^2, and the distance between the probe electrodes is 1.4 cm.

The conductivity is essential for the electrodes to obtain the bioimpedance and the cardiac signal. It is observed that the electrodes created with nozzle's temperatures of 140 °C and with the heated bed temperature variation of 40 °C and 110 °C are the two electrodes with lower resistance or higher conductivity. From the data obtained from the temperature and its relationship with the resistance measurements, the b40t140 and b110t140 labels are used for further measurements.
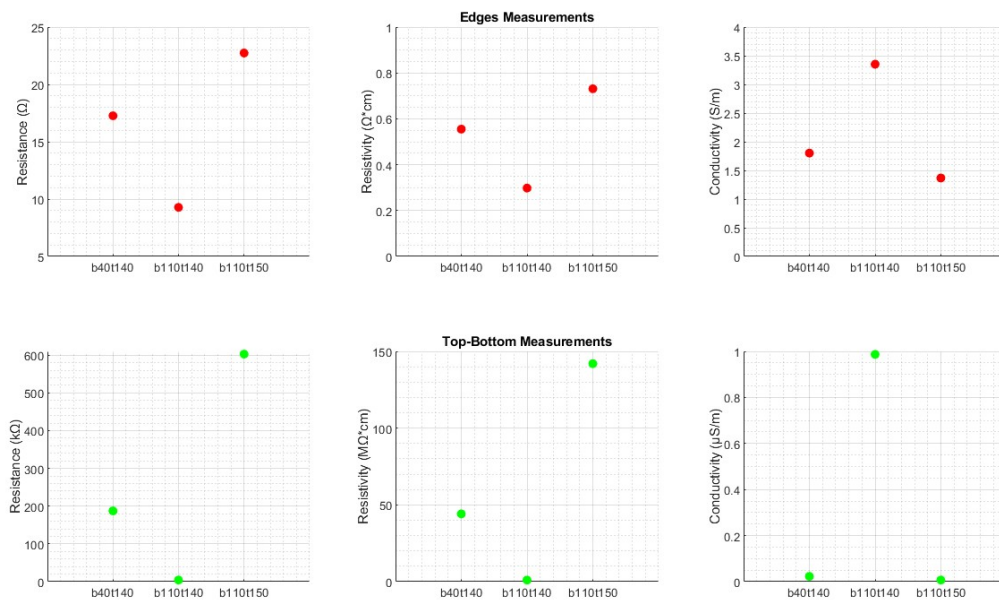
Figure 5.3: The effect of temperature on the electronic characterization (Resistance, resistivity and conductivity).

5.2 Fabrication of Dry Flexible Electrodes

The design and creation of files for 3D printing corresponding to the diameters 7 mm, 15 mm, 23 mm, and 30 mm with thickness of 0.3 mm were carried out. The table 5.3 shows the area of contact of the electrodes to further comparation with the state of art.

Table 5.3: Area of the electrodes

Area (mm^2)	39	177	415	707

The figure 5.4 shows the respective designs made in the SolidWorks program with the 3D printing conditions of the PrusaSlicer program. The print was configured for two different temperatures (heated bed temperature: 40 °C and 110 °C), which were selected in the previous section.
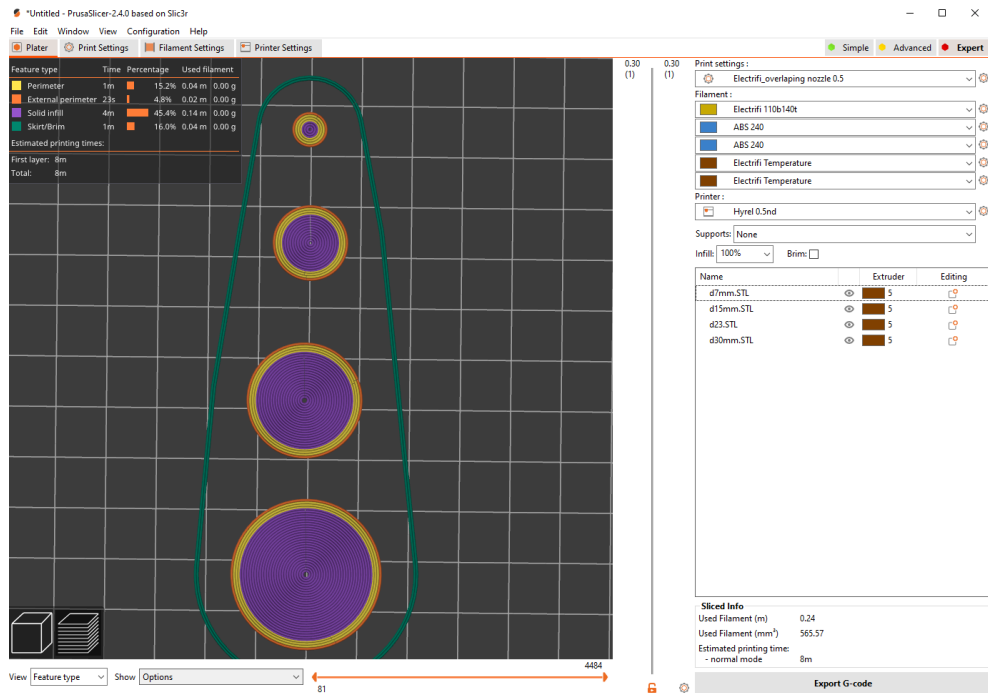
Figure 5.4: Electrode design from top to bottom, 7 mm, 15 mm, 23 mm and 30 mm.

With the G-codes programmed for each electrode, the obtained electrodes are shown, with the different contact surfaces with the skin. The figures 5.5 shows the electrodes printed with Electrifi, already connected to the cables for the electrical characterization.
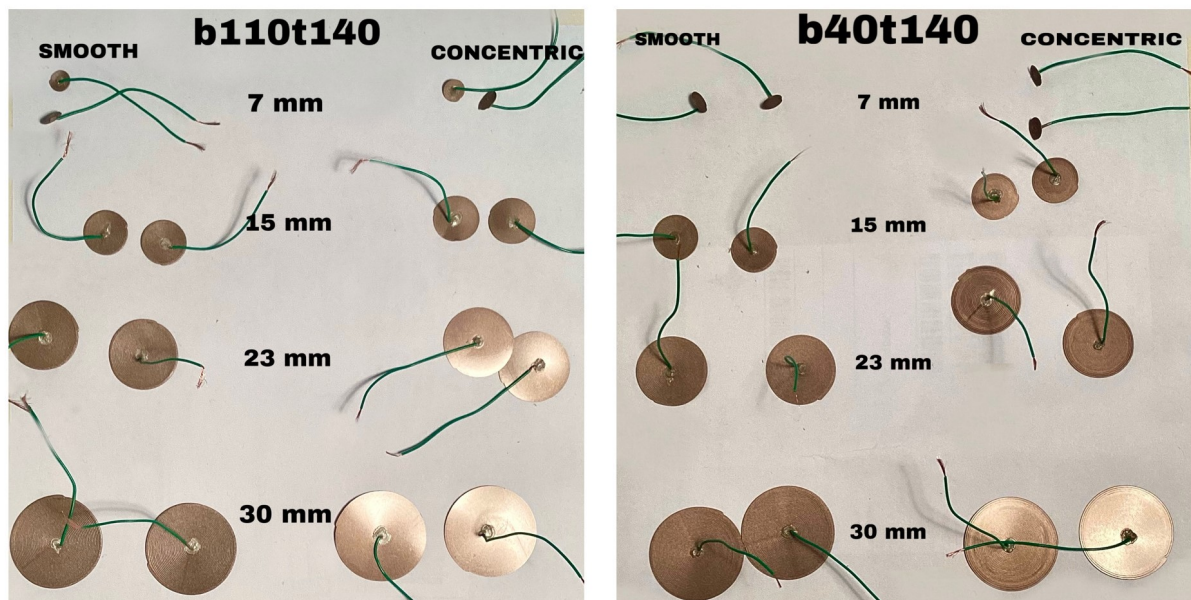
Figure 5.5: Electrodes with 7 mm, 15 mm, 23 mm, and 30 mm labeled b110t140 and b40t140 with a smooth and concentric textured contact surface.

Texture of the Skin Contact Surface

To compare the electrodes of b40t140 and b110t140, the contact texture "concentric" shows the concentric trajectory of the patern with which the 3D printer prints. However, it shows more relief for the concentric texture of b110 than with b40. While for the "smooth" texture, the path of the electrodes is much less visible than the "concentric" one, making it more uniform and without relief. It is observed that this type of texture does not show the trajectory when using the b110t140 compared to the b40t140. The figure 5.6 shows the texture "smooth" and "concentric" of the electrodes with 30 mm diameter. The material's characterization was carried out to understand better and observe the differences in the textures of the electrodes' contact surfaces.
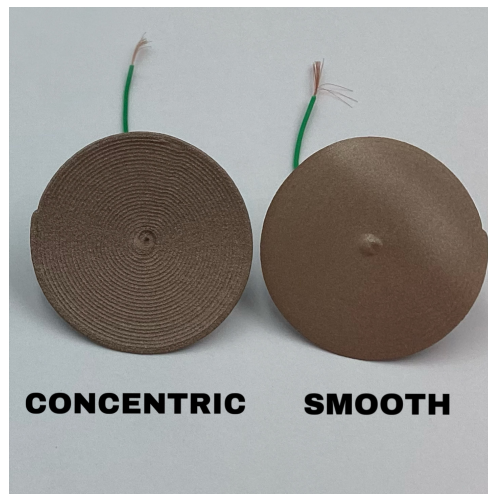
Figure 5.6: The texture "smooth" and "concentric" of the electrodes with 30 mm diameter.

Flexibility

The flexibility experiment showed that electrodes from the slightest 7mm to the largest 30 mm can be easily bent and twisted with the fingers.It is seen that the bending and twisting of the electrodes are carried out without causing their rupture or deformation. The figure 5.7 shows the bending and twisting of the electrode with a 23 mm diameter.

Figure 5.7: Twisted and Bended to a 23 mm diameter electrode.

5.3   Material Characterization

5.3.1   Stereomiscroscopy

Stereomicroscopy showed how when the filament is melted with a heat bed temperature of 110 °C, the deposition is more uniform, and for both the smooth and concentric textures, the lines of the printing pattern are not as visible as with the temperature of 40 °C. The figure 5.8 shows the photos obtained with the stereomiscroscope for the 15 mm diameter electrode.
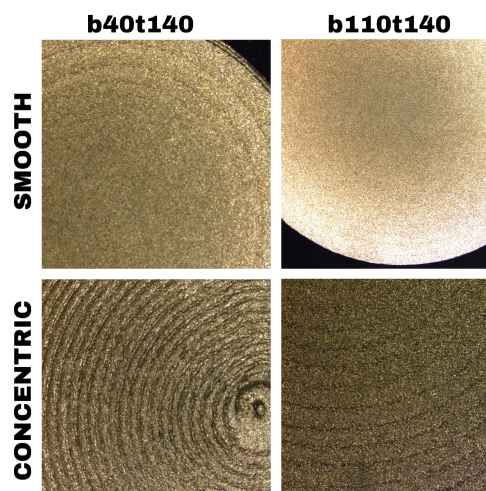
Figure 5.8: Stereomiscroscopy of the 15 mm diameter electrodes.

SEM Spectroscopy

The SEM Spectroscopy figure 5.9 showed how the deformation and irregularity of the deposition of the material are more significant in the heated bed temperature of 40 °C compared to that of 110 °C. For 110 °C the deformation is visible, but also the surface more regular and without cracks. On the other hand, in the SEM Spectroscopy figure 5.10 for the smooth texture, the temperature of 40 °C and 110 °C does not show irregularities or textures. However, you can see small lines or patterns in the heated bed temperature of 40 °C.
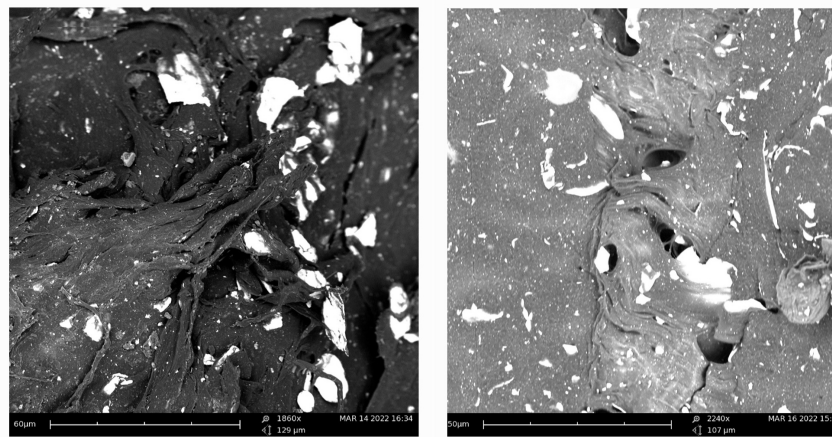
Figure 5.9: SEM Spectroscopy of the concentric contact surface of the 15mm diameter electrode. The left figure shows the 40 °C bed heated temperature, the right figure shows the 110 °C bed heated temperature.
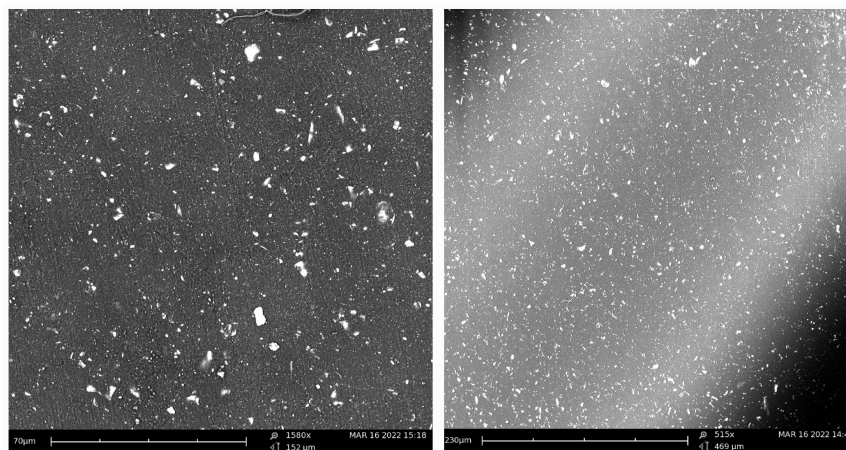
Figure 5.10: SEM Spectroscopy of the smooth contact surface of the 15mm diameter electrode. The left figure shows the 40 °C bed heated temperature, the right figure shows the 110 °C bed heated temperature.

5.3.2   Profilometry

The profilometry was carried out for the 15 mm diameter electrodes for the texture of the "Smooth" and "Concentric" contact surface. The figure 5.11 shows that for the smooth texture when the heated bed temperature is 110 °C, minor relief is shown than with a temperature of 40 °C. This is because at high temperatures, the filament melts, and its deposition is much more compact. On the other hand, in the profilometry of the concentric texture, it is observed that there is a pattern of peaks in the electrodes with a temperature of 40 °C and 110 °C. However, this pattern is repeated more times in the 40 °C electrode.

Likewise, the figure 5.12 is shown that there is more texture and irregularities in these repeating patterns compared to those shown in the 110 °C temperature electrodes. These cycles are shown as they are printed with a concentric pattern, which is more visible when you have a low temperature than when the material melts. In addition, as with the smooth texture, melting the filament for 3D printing makes its deposition much more uniform and compact.In addition, with the profilometry, it is observed that the material sags when a temperature of 110 °C is used for the printer's heated bed. For the smooth texture, the electrode shows buckling on the left side, while for the concentric texture in the center of the electrode.
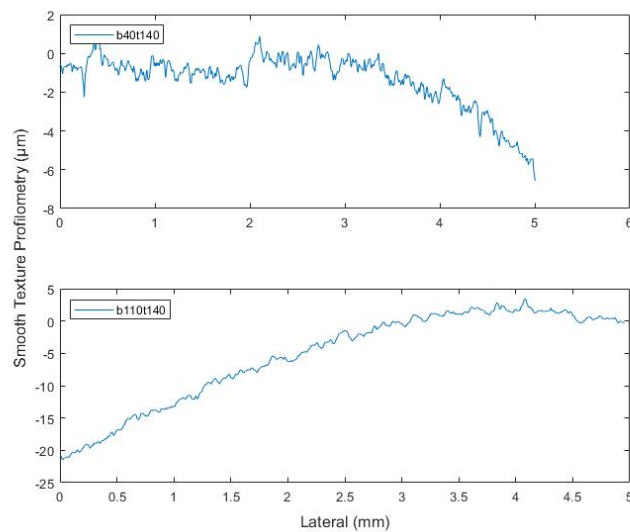
Figure 5.11: Profilometry of the Smooth texture of 15mm electrode
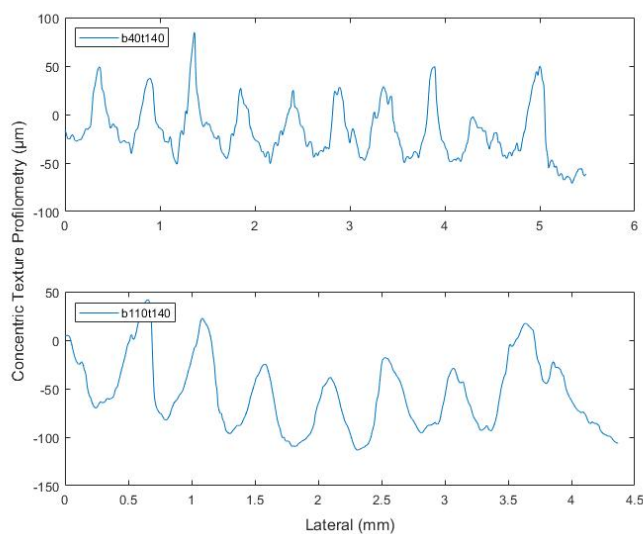
Figure 5.12: Profilometry of the Concentric texture of 15mm electrode

5.4 Frequency Response of Electrodes: Diameter, Texture and Temperature Research

The figure 5.13 shows the stable electrode impedance over the entire frequency range for the 30 mm, 23 mm, and 15 mm electrodes. As [100] when performing the impedance of the electrodes between their top and bottom, impedance without change concerning the applied frequency should be obtained. In both figures, the only electrode that does not meet the stability over the frequency is the 7mm one, and the changes are shown at low frequencies. This may be due to human error, and the electrodes are too small and do not hold together across their entire surface.
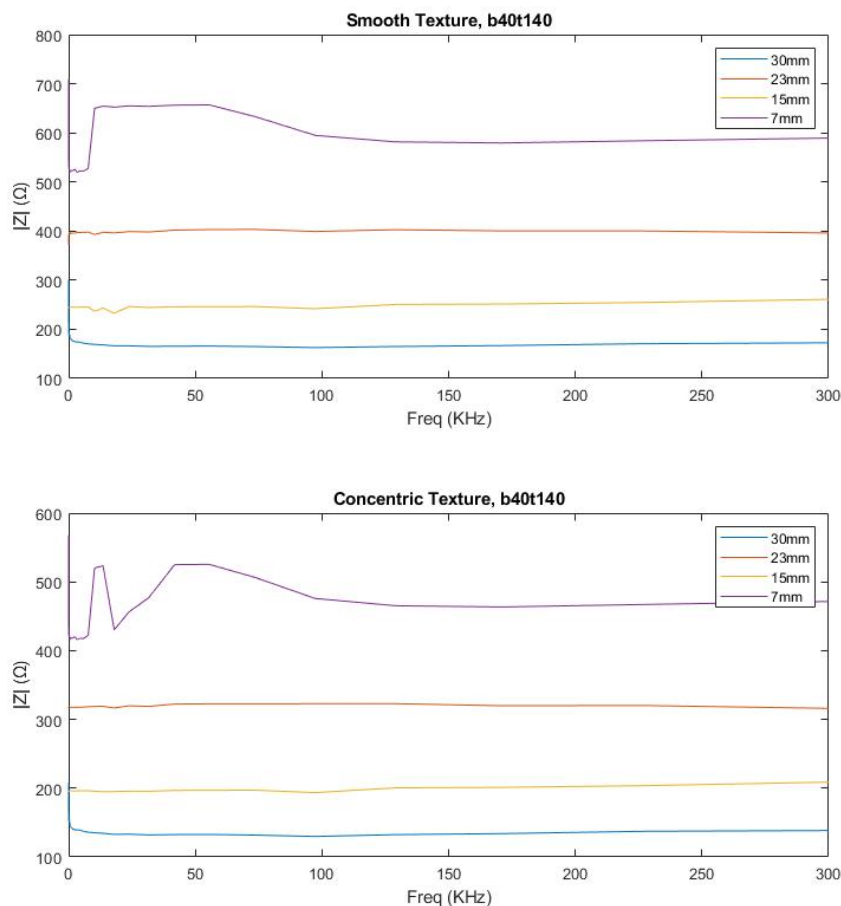
Figure 5.13: Frequency response of the b40t140 electrodes.

The figure 5.13 shows the impedance when the concentric textures are in contact shows a lower impedance than the smooth texture. It is observed that the electrodes with the lowest impedance are those of 30 mm in diameter (concentric with an average impedance of 165.84 nm and smooth of 209.83 nm). However, at low frequencies ($\approx$10Hz), a drastic increase of $\approx$300nm is shown for the concentric and smooth texture. For the 23 nm and

15 nm electrodes, it is where the most constant impedance is observed over the frequency.
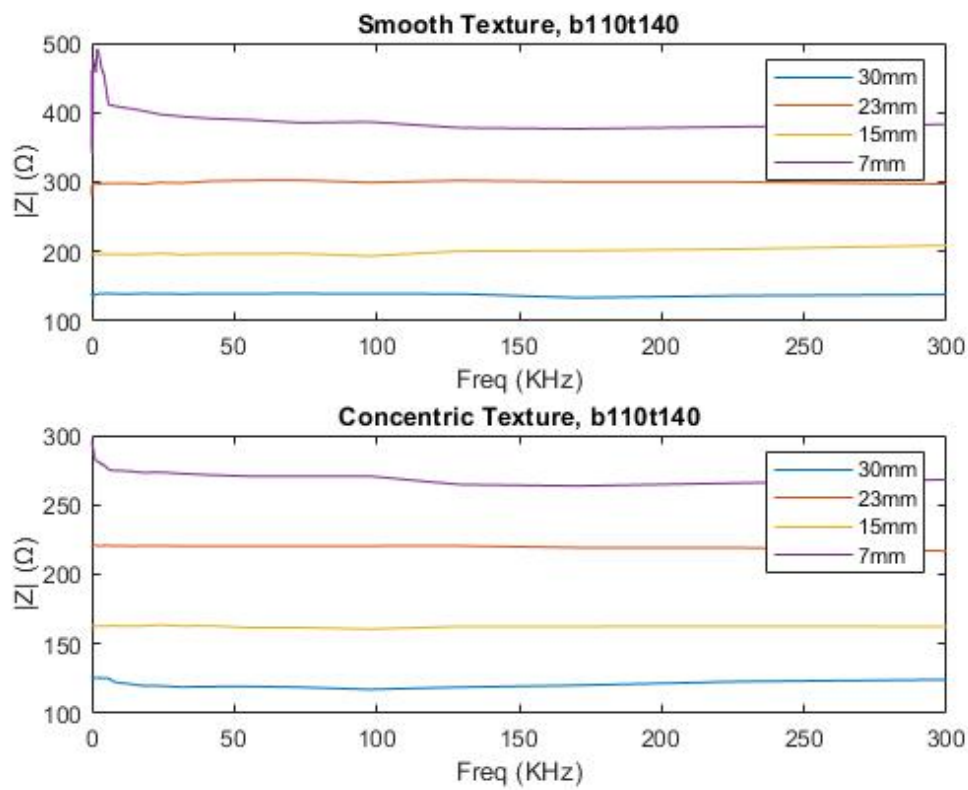
Figure 5.14: Frequency responde of the b1100t140 electrodes.

The figure 5.14 shows the frequency response of the electrodes when contacting the smooth and concentric surfaces for the electrodes with the label b110t140. Electrodes with heated bed temperature 110 °C obtained better results with a lower impedance than 40 °C. The 23 mm and 15 mm electrodes remain stable over the frequency, while the 7 mm electrodes show a rise in frequency (less than 10 Hz). Although the 30 mm electrodes obtained lower impedance, they are not as stable as the 15 mm and 23 mm ones. Likewise, with the b40t140 electrodes, it is shown that the concentric texture is the one with the lowest impedance, with 162.39 Ω for the 15 mm diameter electrodes and 220.32 Ω for the 23 mm diameter electrodes.The average impedance of the electrodes that were kept constant are summarized in the table 5.4.

Table 5.4: Impedance of the stable electrodes

Label	Impedance |**Z**| (Ω)			
	15 mm Smooth	15 mm Concentric	23 mm Smooth	23 mm Concentric
b40t140	244.950	196.218	392.365	312.533
b110t140	196.292	162.396	294.337	220.324

5.5 Skin-Electrode Impedance: Diameter and Texture Research

5.5.1 Overtime Stability

The figure 5.15 and 5.16 shows the results of the time dependence of the electrode-skin impedance. The constructed dry electrodes decrease over time. As expected, the Ag/AgCl gel electrodes generate the lowest impedance and are stable all over the experiment. The impedance measured with the wet electrodes is around 340 Ω. In contrast, from lower to higher impedance measurements, they are the electrodes of 30 mm, 23 mm, 15 mm, and 7 mm, that is, inversely between the impedance and the contact area.

Two graphs were made to compare the dependence of the stability time with the contact structure of the electrodes. It is observed in the figure 5.15 of the "b110b40" smooth texture of the electrodes that at the frequency of 100 kHz, at approximately 20 minutes, the values of the dry electrodes are relatively stable, saying that they reached their saturation state. While for the "b110b40" electrodes with the concentric texture (Figure 5.16), they became stable at around 25 minutes. However, the 7 mm electrode with concentric texture present a drastic declay 25 minutes. As well, it can be seen that the values obtained are less stable than the values obtained with the smooth texture. It is observed that the electrodes with smooth texture obtained lower values than the concentric ones. However, this values will be deepened in the continuing sections.
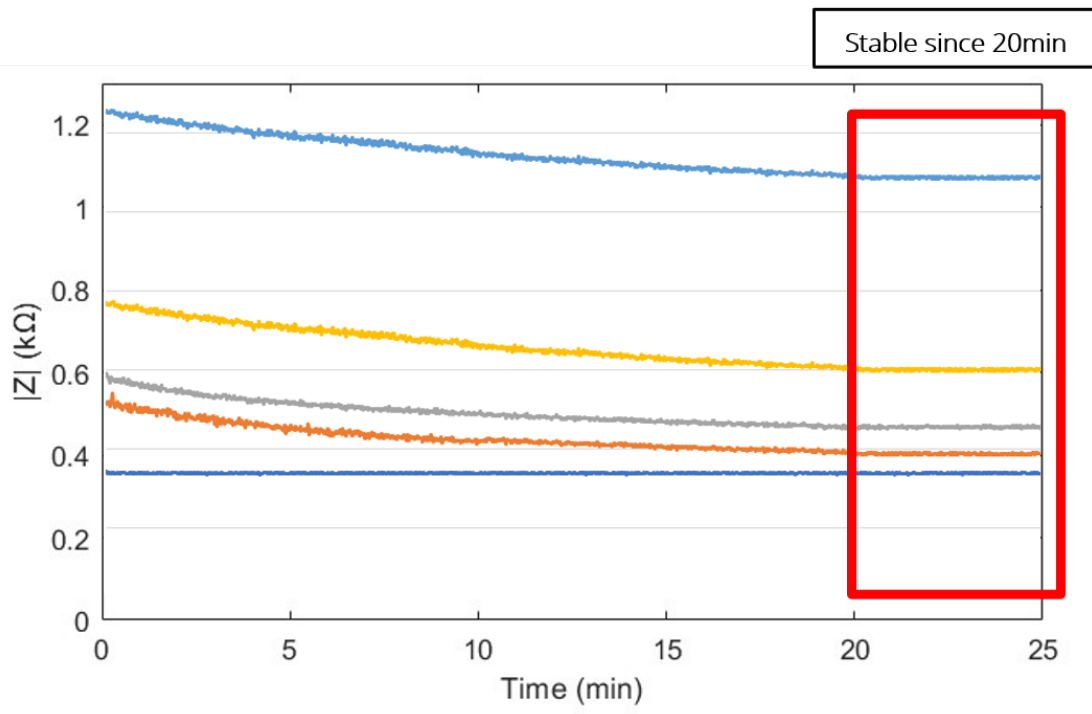
Figure 5.15: Time Dependency of the dry and wet Electrode-Skin Impedance - Smooth texture
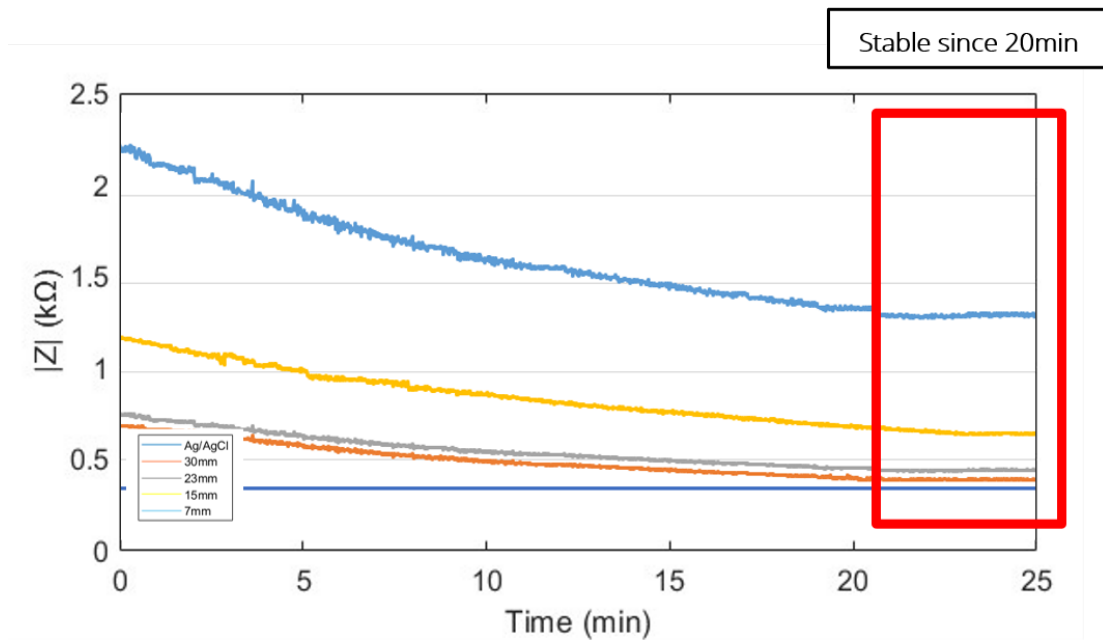
Figure 5.16: Time Dependency of the dry and wet Electrode-Skin Impedance - Concentric texture

Therefore, to obtain the impedance values of the saturation state (the lowest), the following experiments were carried out 30 minutes after the electrodes were placed.

5.5.2 Skin Adhesion of the dry electrodes

Micropore Medical Tape to adhere to the skin and its relation with skin impedance measurements

The figure 5.17 shows the frequency dependence in the results of the skin-electrode impedance with the smooth contact texture. As expected, the Ag/AgCl wet electrodes lead to a very low impedance (around 2.5 kΩ - 3kΩ) and constant over frequency. In contrast, dry electrodes do show a frequency dependency of skin impedance. It is observed that the electrode with a diameter of 30 mm is the one with the lowest impedance among the dry electrodes. Additionally, it is emphasized that the 7mm electrode is the most unstable and has a much higher impedance (9 MΩ) than the other dry electrodes -around 53 times greater than the 30 mm electrode at the 0.1Hz frequency-, therefore it is discarded for the following experiments and is downplayed in the figure.

The right graph from the figure 5.17 shows the previous graph but focuses on the frequency range of 2.5 - 300 kHz. It is observed that the dry electrodes of 15 mm, 23 mm, and 30 mm obtain lower impedance (667 Ω, 358 Ω, 257 Ω respectively) at high frequencies compared to the stable impedance of the wet electrodes (2.8 kΩ).
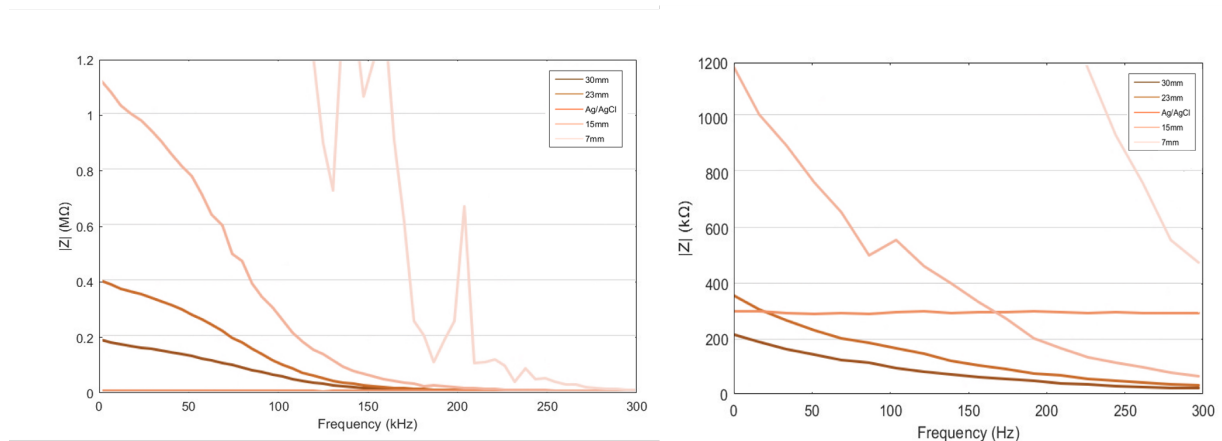
Figure 5.17: Frequency Dependency of the dry and wet Electrode-Skin Impedance - Smooth texture "b110t140", right graph is zoomed

The dependency over the frequency of the concentric texture (Figure 5.18) is similar to that of smooth. However, the values obtained are higher than with the smooth. Likewise, the high frequencies (20 kHz-300 kHZ) values remain lower than the constant impedance obtained by the Ag/AgCl wet electrode (2.8 kΩ). The impedance values of the dry electrodes (7 mm) are much higher, reaching a maximum value of 22 MΩ at 0.1 Hz frequency and a minimum value of 23 kΩ at 300 kHz; therefore, this electrode is discarded for the following measurements.
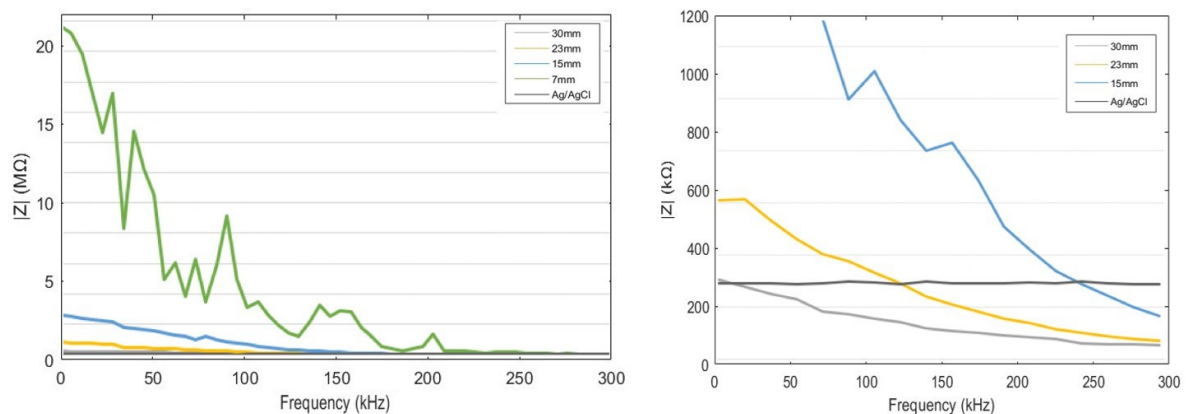
Figure 5.18: Frequency Dependency of the dry and wet Electrode-Skin Impedance - Concentric texture "b110t140", right graph is zoomed

The figure 5.19 showed that the trend from lower to higher impedance are the electrodes of 30 mm, 23 mm, 15 mm in order. In the case of printed electrodes with a heated bed temperature of 40 °C, this is not the exception. However, when performing the experiments with the electrodes labeled "b40t140", the impedance results in the skin are higher than the results obtained with "b110t140". For a better understanding of the difference in impedance measured between the two types of electrodes, see the table 5.5:
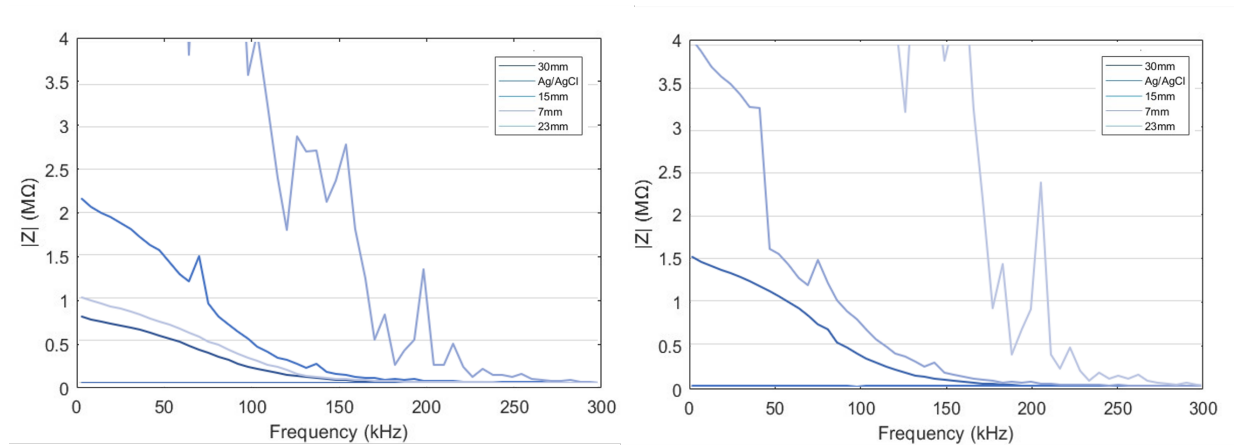
Figure 5.19: Frequency Dependency of the dry and wet Electrode-Skin Impedance - Smooth (left) and Concentric (right) texture

Table 5.5: Skin-electrode impedance summarize at 0.1k, 2k and 300k Hz (freq)

freq (kHz)	Diameter (mm)	b110t140 Smooth (kΩ)	b110t140 Concentric (kΩ)	b40t140 Smooth (kΩ)	b40t140 Concentric (kΩ)	Ag/AgCl wet electrode (kΩ)
0.1	30	184.04	797.48	552.11	1049.00	2.97
	23	398.74	2572.27	797.48	1515.21	
	15	1118.38	21665.42	2236.76	4070.90	
2	30	2.19	6.10	6.56	9.84	2.92
	23	3.59	27.32	7.18	9.34	
	15	11.88	1327.60	23.76	30.89	
300	30	0.26	0.56	0.77	1.01	2.91
	23	0.36	0.72	0.72	0.93	
	15	0.67	1.67	1.34	1.74	

From these results, the other tests will be carried out to compare with the best electrodes in this experiment, the dry electrodes with label "b110t140" smooth texture as contact surface.

Applied force and its relationship with skin impedance measurements
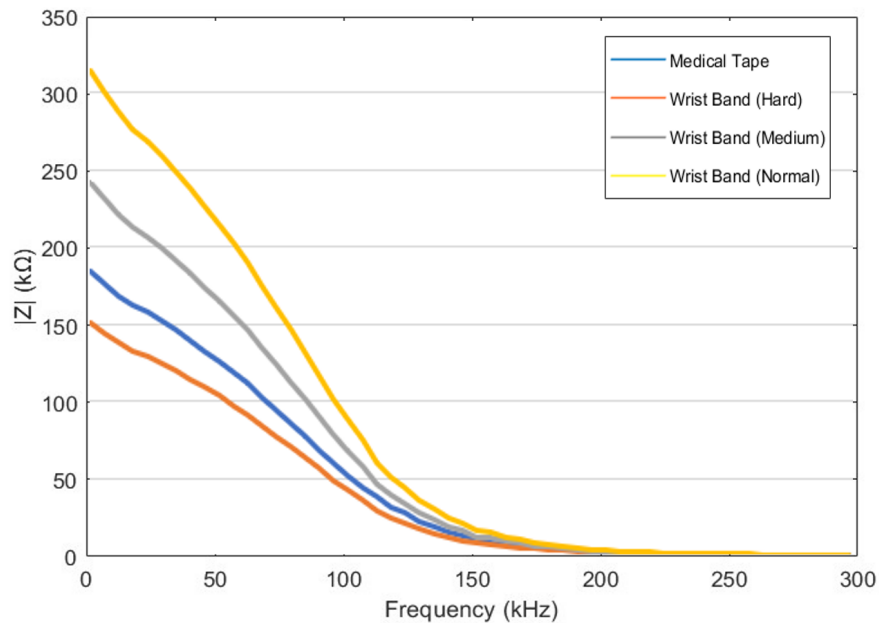
Figure 5.20: Applied force and its relationship with skin impedance measurements

The figure 5.20 compares the impedance with the skin if pressure is applied between the electrode and the skin. The electrodes that were study were the 30 mm diameter. It is observed that when the wrist band is used, squeezing it tightly or "hard" level (taking care not to cut off the circulation), lower impedance values are obtained than when the medical tape is used (247 Ω vs. 257 Ω at 300 kHz and 150 kΩ vs. 184 kΩ at 0.1 kHz, respectively). However, when placing the wrist band tightening it at a "medium" level and a "normal" level where no additional force is applied to that exerted by the band, the impedance measurements are greater than those obtained with the medical tape.

Skin preparation and its relation with skin impedance measurements

The figure compares impedance when skin-electrodes are measured on skin moistened with body cream before measurement. The electrodes chosen to do this measurement were just the 15 mm, 23 mm and 30 mm, the ones that show uniform over the frequency impedance in the previous section. It is observed that the results obtained when moistening the skin are lower than when the skin is dry. However, it is observed that the measurements made on moist skin do not have a consistent trajectory despite dependence on the frequency. The table 5.6 shows the comparison of the values at three frequencies (300 kHz, 3 kHz, and 0.1 Hz)
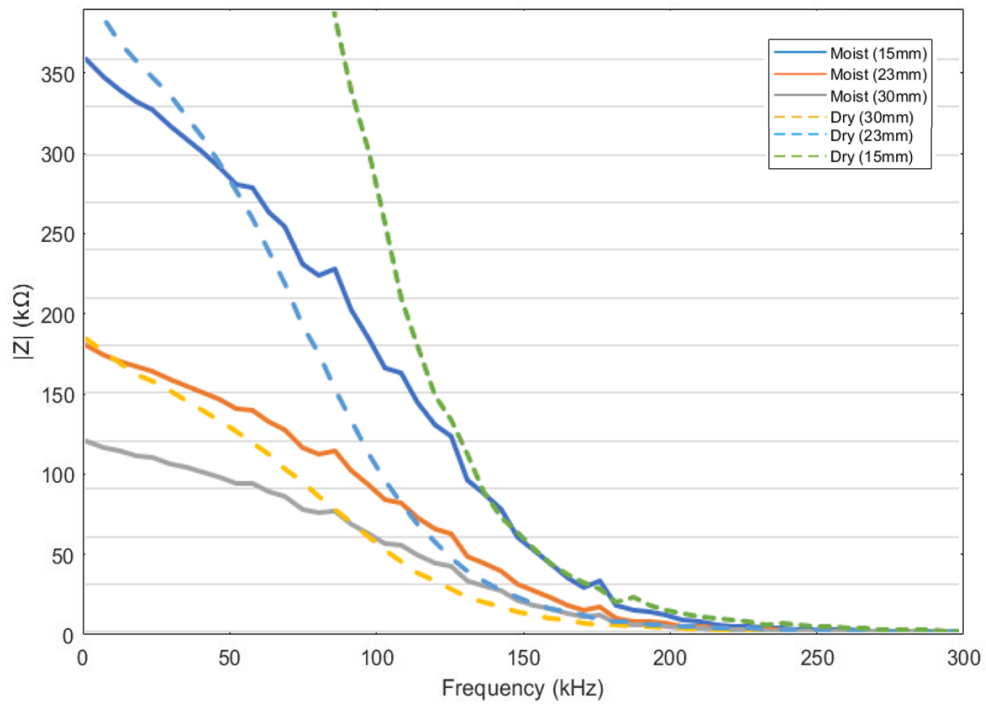
Figure 5.21: Moisturization and Dry skin for Skin-Electrode Impedance Measurements

Table 5.6: Skin-electrode impedance summarize for [0.1k, 3k and 300k] Hz (freq) for dry and moist skin

freq (kHz)	Diameter (mm)	Moist skin Impedance (kΩ)	Dry skin Impedance (kΩ)
	30	119.75	184.04
0.1	23	179.62	398.74
	15	359.24	1118.38
	30	74.62	94.84
3	23	111.93	192.03
	15	231.02	493.29
	30	0.20	0.26
300	23	0.28	0.36
	15	0.59	0.67

Finally, it should be noted that at the end of the tests carried out, the electrodes did not show any deterioration or damage to the visible surface structure. Using light cream

to moisturize the skin does not leave a heavy or visible residue on the electrodes. However, the electrodes are cleaned before each test with alcohol and dried at room temperature.

5.6   Electrocardiogram Measurements

5.6.1   Hardware and Software

The electrical connections described in the methodology 4.5.1 were followed to connect the ECG modules, each one to its own Arduino, and connected to the computer's COM3 and COM4 ports.

In the LabVIEW software, the configuration is made to acquire the ECG signal with the two electrodes simultaneously. The graphic programming carried out both to establish communication between the computer and the Arduino devices are shown in the figure 5.22 and 5.23.
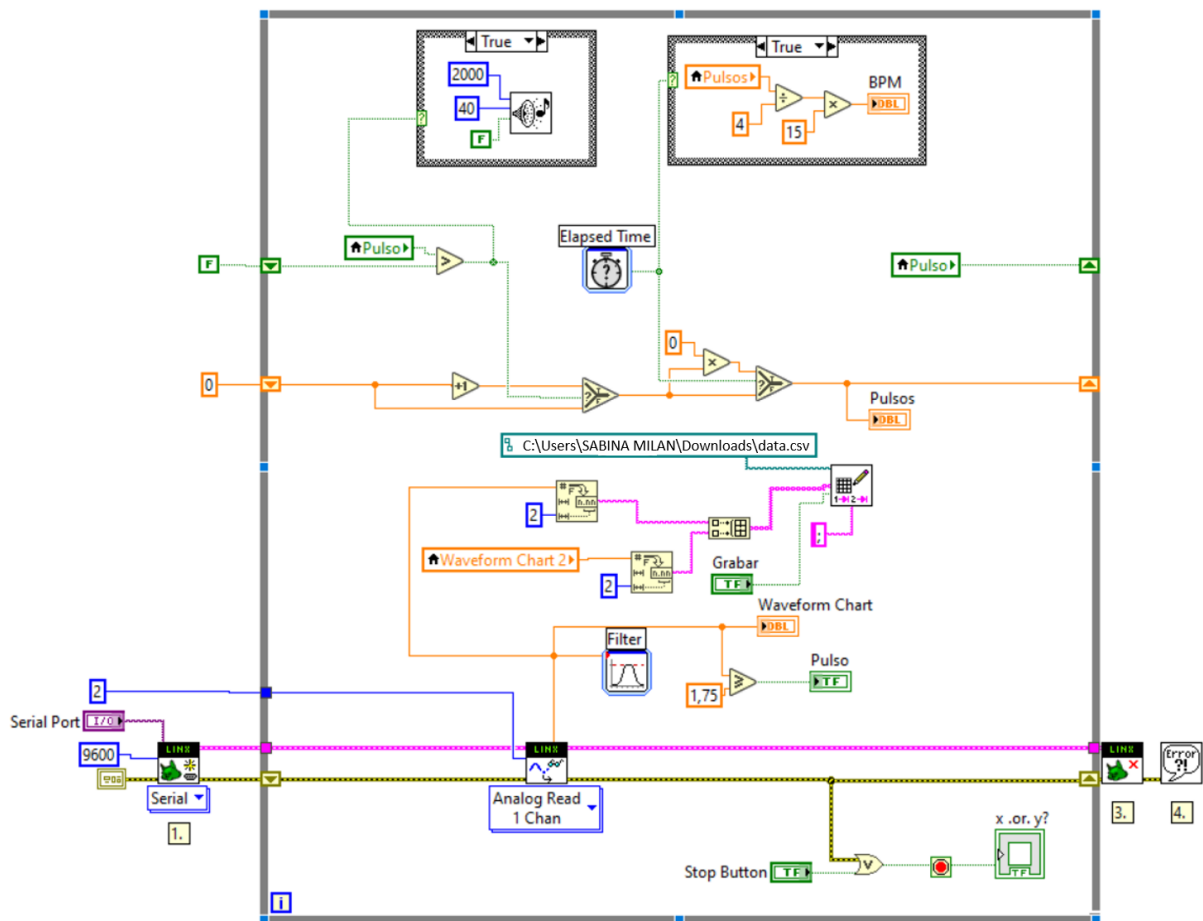
Figure 5.22: Graphic programming to cardiac signal adquision with dry electrodes (developed in this thesis)

It is observed that the sensor delivers the signal obtained and is controlled by one of the channels. In the upper part (the green section), a sound is played every time a

complete QRST cycle occurs -as shown in the image when the pulse variable is greater than a certain value- which works with 40 Hz and 2000 of tone to be able to represent the most similar to an electrocardiogram sound used in clinics. An elapsed time is also given, which is the delay time because the acquisition of the signal is not one hundred percent in real time since it takes time between measuring and sending the data. The elapsed time is around 15 milliseconds. On the other hand, to have a similarity between the voltage values obtained, an evaluation is made between the pulse received and the past one to smooth the signal. Additionally, in the upper right part (in orange), you can see the internal calculation carried out by LabVIEW to give an estimate of the beats per minute. If we look at the central part, we can see the path where the data will be saved. Finally, a STOP button was configured, which broke the Arduino and computer connection to end the cardiac measurement.
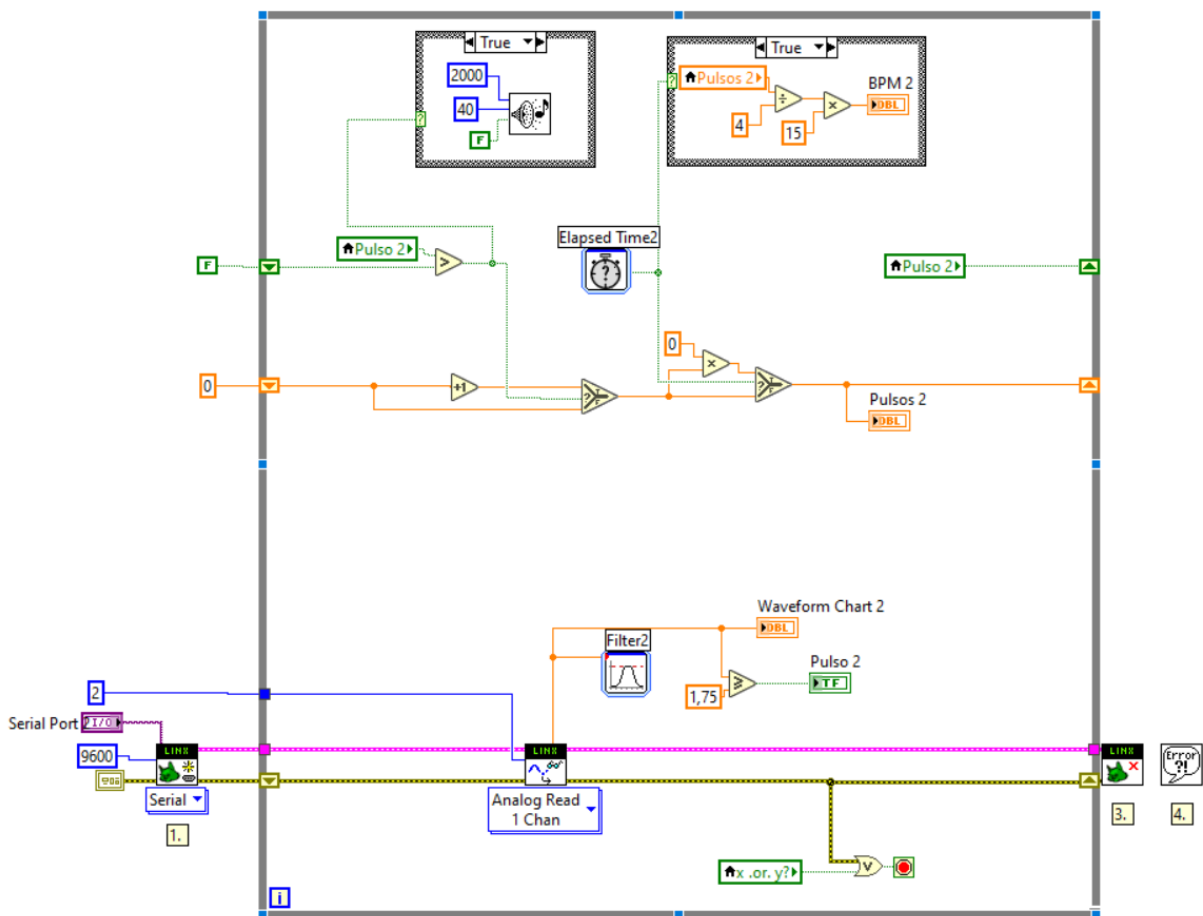
Figure 5.23: Graphic programming to cardiac signal adquision with wet commercial electrodes

The second picture describes the configuration for obtaining data using commercial electrodes. Additionally, note that these two photos show the entire configuration, which works in parallel. However, it is remarkable the presence of a filtering step; however, it was only used as a test since the ECG module contains its filters explicitly used to improve the acquisition of the cardiac signal. In the end, all the filters placed in the configuration

were disabled.

The figure 5.24 shows the interface (Front Panel) of the LabVIEW software; in this part, it is visible the USB ports to which the two Arduino are connected (COM3 for developed dry electrodes and COM4 for commercial wet electrodes), it should be noted that although these USB ports are used, the communication between the Arduino devices and LabVIEW is serial but this does not affect in any way the speed of data acquisition and the resolution of these signals. In addition, there is a green-grey bottom that says recording. The moment the bottom is pressed, it has a delayed time but starts to save the data in the CSV file.
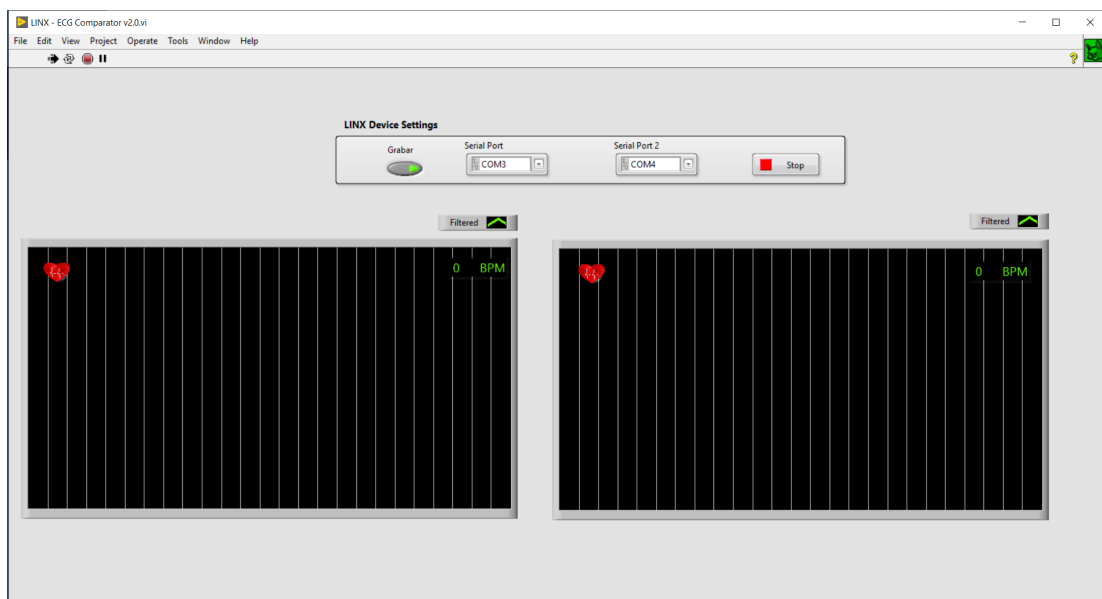
Figure 5.24: Interface of the electrocardiogram developed

The figure 5.26 shows an example of cardiac signal acquisition; on the right is what is obtained by the developed dry electrodes, and on the left is the commercial wet electrodes. The image shows the interface operating the programmed and configured electrocardiogram. Something to emphasize is that the bpm obtained is calculated by the developed program: counting the cardiac cycles that the person has in 15 seconds and multiplying by four. The value is an approach.

Figure 5.25: ECG signal obtained example

5.6.2 ECG signal

The figure is presented where the rest state position of the test subject is observed, in addition to the placement of the electrodes. The study subject is a 33-year-old male adult who maintains an active state of exercise but is not considered an athlete. This is mentioned to have a defined range of the bpm obtained.

Figure 5.26: Subject with the SetUp of the ECG

After performing several tests for the correct use and management of the acquisition of the cardiac signal, the following signs are received in parallel. Additionally, it is to divide

the pulse reading by four and multiply their output by 15; that is, measure the frequency every 15 seconds and obtain a bpm value that is as up-to-date as possible.

The figure 5.27 shows the signal obtained in a 120-second trial, where it was received with the data for the dry electrodes in a range of 0 to 2.5 mV, while for the data obtained by the commercial wet electrodes, the values obtained are between 1.6 to 1.9 mV. It can be seen a constant line at the beginning of the measurement (highlighted in a square) which is the time (around 13 seconds) that was decided to stabilize the data before recording it. Additionally, the measurements acquired with the dry electrodes created in this thesis show higher voltage, which can be related to the fact that the contact area with the skin is bigger than with the commercial wet electrodes.
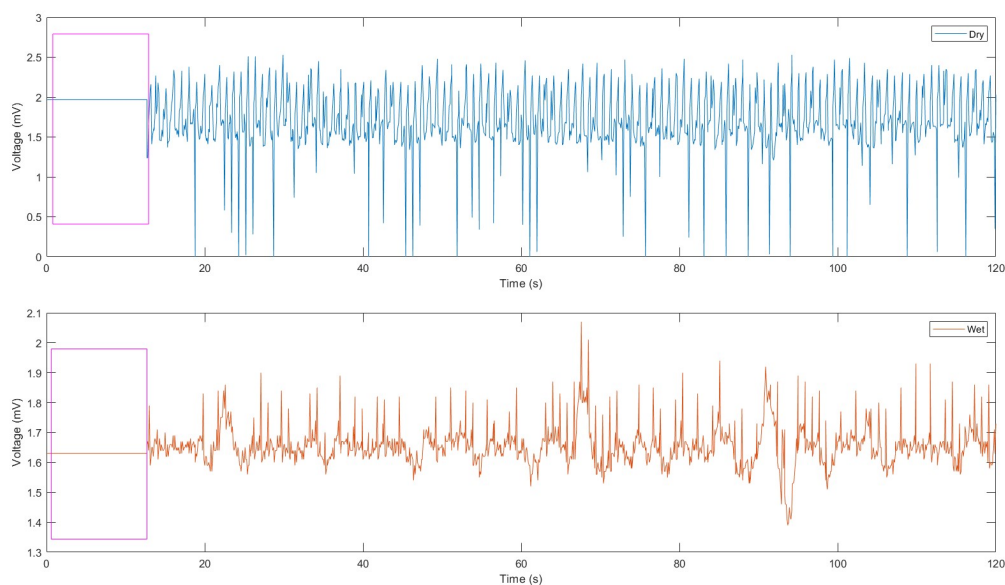
Figure 5.27: Cardiac measurement was performed for 120 seconds, dry electrodes in the figure above, and wet electrodes in the figure below.

The figure 5.28 shows the peaks obtained in 9 seconds; precisely for this section, a value of 65 bpm was obtained for the commercial electrodes, while for dry measurement, it yielded a value of 72 bpm. However, throughout the measurement, bpm values were obtained in a range of 60 to 66 bpm for commercial electrodes, while values between 69 and 80 bpm were obtained for the use of dry electrodes.

Comparing the signals obtained between the two types of electrodes, it can be said that with the dry electrodes developed in this thesis, higher voltage signals were obtained, making noise less influential in these measurements. Likewise, there is a desire that, in some cases, can reach 0 mv on the y-axis, which is related to the fact that the connections of the electrodes and the cables are not 100% stable. Additionally, the noise was obtained, much more noticeable as it does not follow the previously acquired form; this is because the system developed to receive the cardiac signal is very sensitive to the person's movement. It was tried not to move at all; however, minimal movements decreased the signal.
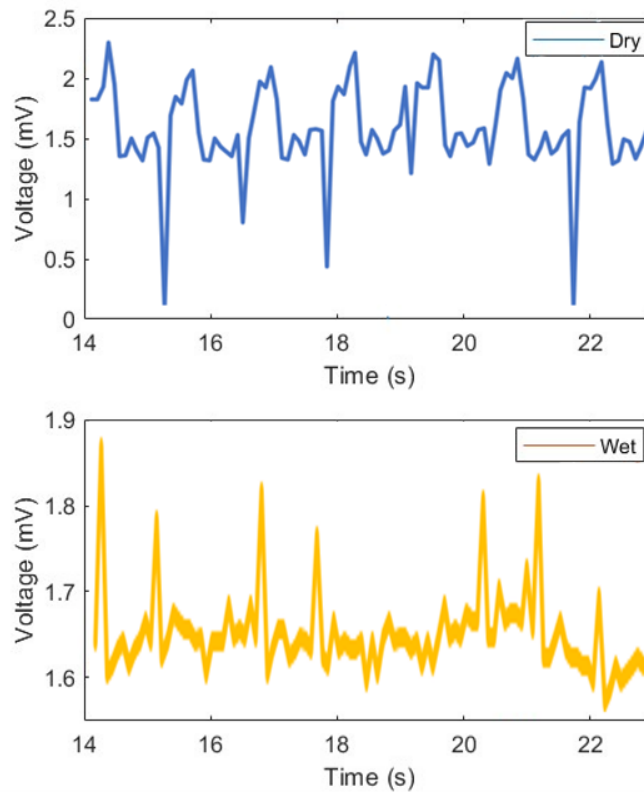
Figure 5.28: Cardiac measurement, 9 seconds record.

The figure 5.29 shows the characteristics of the cardiac signal, such as the QRS complex, P-wave, and T-wave observed in the signal acquired with commercial wet electrodes. However, when acquiring the cardiac signal with the dry electrodes, the P-wave cannot be identified, and the R-wave shows a not stable peak.
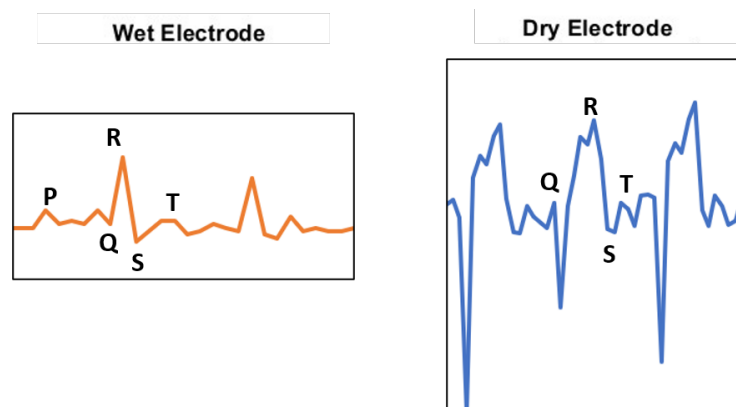
Figure 5.29: Cardiac Cycle

5.7   Effect of the dry electrodes on the skin

After performing the experiments, the reactions in the skin when using the dry electrodes. The figure 5.30 shows the dry electrodes were placed for 30 minutes for the impedance measurements over the frequency, where the dryness of the skin (in white) due to the micropore medical care is observed. However, where the electrode was placed with the smooth contact surface presents a greater production of sweat from the skin than the concentric texture.
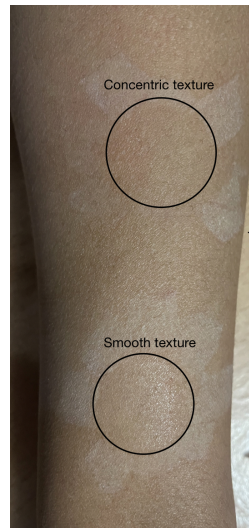
Figure 5.30: Effect of the dry electrodes (concentric and smooth) on the skin

Chapter 6

Discussion

The dry electrodes printed in a 3D machine with the Electrifi filament were tested during the development of this thesis. The printing temperature was one of the aspects to experiment with in developing this thesis. Some works related to microstrip transmission lines or path antenna, development of components, and circuits have been created with this filament; however, no work has been published in the biomedical area. Despite being works from different areas, they were developed under 3D printing; Ray et al., manage the temperature of the printer nozzle at 145 °C with a speed of 10 mm/sec and an infill of 100%. Likewise, the author uses a paste like the industrial silver epoxy to increase the conductance. In the development of this thesis, the nozzle temperature was used at 140 °C (the same used in Flowers et al.), giving favorable results since at higher temperatures, the resistance increases [101]. Likewise, a low printing speed was maintained due to the delicacy of the material and the pressure that is needed. However, when using the conductive paste, the author let it rest for 24 hours, which is different from what is mentioned in the results section. This is because there is a difference between the paste used to fabricate the electrodes and the trace ([101]), and each one has a different drying time recommended by the manufacturer.

According to Flowers et al., the impedance obtained when working with Electrifi which has 3 Ω -resistence described in the data sheet- is lower compared to other materials such as Proto paste (1.2 kΩ) and Black Magic (100 Ω) [102]. Hence, the objective of this thesis is to introduce this conductive material to the medical area. Likewise, in Flowers et al., It is shown that in the bending test performed on the electrifi filament, the resistance varies in the range of 10-15 Ω and does not break even after 500 bending cycles [102]. In this thesis, flexibility is tested by bending and twisting each developed electrode without observing a change in the structure of the developed electrodes.

After the temperature study, the manufacture of the dry electrodes was carried out, and the frequency response of electrodes was experimented with like in Kusche et al., who manufactured five different electrodes (gold-plated, stainless steel, carbon rubber with smooth surface, carbon rubber with surface textures and conductive [100]. The impedance obtained in the range from 24 kΩ to 400 kHz by [100] is stable all over the frequency, as the results from the electrodes (diameter = 30mm, 23mm, and 15mm) developed in this thesis. However, the 7mm was not the case, and maybe because it is too small and the setup used does not fit the electrode's size correctly. The lowest impedance result was

obtained with the 30mm electrode with an approximate value of 150 Ω, which is higher than those obtained with [100]. However, the impedance results obtained in the thesis are higher when smooth textures are put in contact than in texture sides, as observed in [100] with their rubber electrodes.

Following the methodology, the overtime stability of the electrodes was performed where, as expected, the Ag/AgCl gel electrodes generate the lowest impedance and are stable all over the experiment [100]. Kusher et al., carried out this experiment to obtain results where the electrodes present dependence of the impedance with time until reaching their saturation state, which was achieved around 15 minutes. Compared with the results of this thesis, which were obtained in approximately 20 minutes when using the smooth surface of the electrodes than with the textured ones (around 25 minutes). The dry electrodes developed in the thesis need more time to obtain a better adhesion to the skin compared to [100]. However, one factor influencing the difference in time is that the smooth surface better encapsulates the skin, causing it to create sweat faster than with the concentric texture. A picture of it is shown in section 4.5 named "Effect of the electrodes on the skin." The applied force and its relationship with the impedance of the skin were studied, for these measurements were obtained where when applying more pressure, the impedance values decreased, like in the Albulbul et al. where study the electrode-skin impedance changes due to an externally applied force. The measurement where done with wet Ag/AgCl electrodes however, show the same tendency that the more force, the lower the impedance until reaching the saturation state [103]. To evaluate the difference between the moist vs. dry skin impedance measurement, it was shown that the impedance is lower when the skin is moist. This behavior can be explained by the fact that the stratum corneum is hydrated by changing the humidity of the environment between the electrode and the skin. However, the results can be considered ambiguous because the body creams do fulfill their mission of moisturizing, but not all the components are known and how they influence the impedance measurement[104]. The dry electrode adhesion measurements are compared with the results of [12], where dry electrodes (radius= 8mm, 12mm, and 16mm) were created with a conductive MWCNT/PDMS coating to measure skin impedance, and from the heart. It is observed that the behavior of the impedance electrodes has a relationship with the contact areas of each one. The impedance decreased from 1000 kΩ = 8mm, 701 kΩ = 12mm, and 524 kΩ = 16mm at a frequency of 1 Hz as the electrode area increased. For the dry electrodes developed in this thesis, for electrodes with a radius of 7.5mm, 11.5mm, and 15mm at a frequency of 1 Hz, the values are 800kHz, 320kHz, and 150kHz, respectively. Note that the electrode areas in this thesis are smaller than those exposed in [12] and for this reason, the impedance cannot be compared.

Chapter 7

Conclusions

In conclusion, the 3D printing parameters are of the utmost importance to obtaining the desired objectives. In the case of this thesis, working with a conductive and flexible filament led to more care and study of the parameters to be modified for printing. In addition, diameter and surface texture have been studied to obtain the most optimal electrode for cardiac measurement. As a result, flexible bulky dry electrodes were printed with a nozzle temperature of 140 C and 110 C for the heated bed. This parameter was selected given that resistance of 9.3 ohms was obtained and measured from the electrode's edges and 4.3k ohms measured from top to bottom, the lowest resistance among the six different electrodes created.

On the other hand, the frequency response of the electrodes showed that there is stability over the frequency range of 0-300 kHz for electrodes with 15 mm and 23 mm diameter. Additionally, the surface of the electrodes plays an important role because a lower impedance value is obtained when the smooth surface is contacted compared to the concentric one. The lowest and most stable impedance got was 162.4 ohms for a 15mm electrode; however, the lowest impedance was obtained among all the electrodes with a 30mm diameter of around 120 ohms; however, it is not stable throughout the frequency range because the set up with which it was made and the area it manages means that it does not come into precise contact with the surfaces; therefore there may be instability.

After these studies, the tests of frequency response over skin-electrode contact and obtaining the heart signal have been carried out. First, the time the electrodes reach the saturation state has been measured to get the most stable data possible. The studies were conducted at 100kHz, where stability was obtained after 20 minutes of contact between the dry electrodes and the skin. Afterward, skin adhesion and its relationship with impedance were carried out, where the impedance was compared when placing the electrodes with micropore medical tape on dry and moist skin. When placed on moist skin, the results show a difference between 35% at low frequencies and 23% at high frequencies in favor (lower impedance) of moist skin. It is concluded that the frequency response of the skin obtains lower values inversely with the area of contact with the electrodes. In addition to the importance of the structure created on the surface that will be in direct contact with the skin. Finally, it is concluded that increasing the humidity in the environment between

the electrodes and the skin will lower impedance because the skin layers are moistened, reducing their resistance.

Finally, the cardiac signal was acquired, where the software and electrical configuration of sensors were developed to compare the dry electrodes developed in this thesis with the commercial wet ones. It was shown that the p-wave could not be recognized when measuring the signal with the wet electrodes. There were specific unfavorable characteristics at the time of acquiring the signal, such as the developed electrocardiogram system and the connections and adaptations between the electrodes and the cables. In addition, the bpm values obtained with it are higher than commercial wet electrodes. However, the bpm is in the normal range of an adult person in a state of rest and tranquility.

7.1   Future Works

Further research will be focused on the design of the electrodes since different shapes can be obtained thanks to 3D printing, thus working in new structures on the surface that can better adhere to the skin since it has hair, with more presence in men. In addition, it not only works on the development of the surface that will be in contact with the skin but also adapt the electrode so that it adheres easily to the human, such as to clip it to use a clinical electrocardiogram with all the safety towards the person and with the minimal interference of information passing between the electrodes and the electrocardiogram. Thus, to perform the corresponding measurements of skin impedance and cardiac measurements. Likewise, work with a broader study population.

Bibliography

[1] O. S. Soyer, Z. Schofield, G. N. Meloni, P. Tran, C. Zerfass, G. Sena, Y. Hayashi, M. Grant, S. A. Contera, S. D. Minteer, M. Kim, A. Prindle, P. Rocha, M. B. A. Djamgoz, T. Pilizota, P. R. Unwin, and M. Asally, "Bioelectrical understanding and engineering of cell biology," 2020.

[2] "Cardiac muscle and electrical activity — anatomy and physiology ii." [Online]. Available: https://courses.lumenlearning.com/suny-ap2/chapter/cardiac-muscle-and-electrical-activity/

[3] "Health library, body systems and organs, url=https://my.clevelandclinic.org, journal=Cleveland Clinic."

[4] S. Douedi and H. Douedi, "P wave." in *StatPearls*. StatPearls Publishing, jan 2022. [Online]. Available: https://www.ncbi.nlm.nih.gov/books/NBK551635/

[5] Y. Fu, J. Zhao, Y. Dong, and X. Wang, "Dry electrodes for human bioelectrical signal monitoring," *Sensors 2020, Vol. 20, Page 3651*, vol. 20, p. 3651, 6 2020. [Online]. Available: https://www.mdpi.com/1424-8220/20/13/3651/htmhttps://www.mdpi.com/1424-8220/20/13/3651

[6] X. Niu, X. Gao, Y. Liu, and H. Liu, "Surface bioelectric dry electrodes: A review," *Measurement*, vol. 183, p. 109774, 10 2021.

[7] A. Ambrosi and M. Pumera, "3D-printing technologies for electrochemical applications," *Chemical Society Reviews*, vol. 45, no. 10, pp. 2740–2755, 2016. [Online]. Available: http://dx.doi.org/10.1039/c5cs00714c

[8] T. B. Palmić, J. Slavič, and M. Boltežar, "Process parameters for fff 3d-printed conductors for applications in sensors," *Sensors (Switzerland)*, vol. 20, pp. 1–21, 8 2020.

[9] P. The, P. Chomerics, I. To, P. Chomerics, P. Probe, S. Probe, and L. A. W. Ohm, "Surface vs . volume resistivity understanding the two methods and why they matter."

[10] M. J. Deen and F. Pascal, "Electrical characterization of semiconductor materials and devices - review," *Journal of Materials Science: Materials in Electronics*, vol. 17, pp. 549–575, 8 2006. [Online]. Available: https://link.springer.com/article/10.1007/s10854-006-0001-8

[11] R. Kaveh, N. Tetreault, K. Gopalan, J. Maravilla, M. Lustig, R. Muller, and A. C. Arias, "Rapid and scalable fabrication of low impedance, 3d dry electrodes for physiological sensing," *Advanced Materials Technologies*, p. 2200342, 5 2022. [Online]. Available: https://onlinelibrary.wiley.com/doi/10.1002/admt.202200342

[12] A. A. Chlaihawi, B. B. Narakathu, S. Emamian, B. J. Bazuin, and M. Z. Atashbar, "Development of printed and flexible dry ecg electrodes," *Sensing and Bio-Sensing Research*, vol. 20, pp. 9–15, 9 2018. [Online]. Available: https://doi.org/10.1016/j.sbsr.2018.05.001

[13] A. Abdou and S. Krishnan, "Ecg dry-electrode 3d printing and signal quality considerations," *Annual International Conference of the IEEE Engineering in Medicine and Biology Society. IEEE Engineering in Medicine and Biology Society. Annual International Conference*, vol. 2021, pp. 6855–6858, 2021. [Online]. Available: https://pubmed.ncbi.nlm.nih.gov/34892681/

[14] A. dos Santos Silva, H. Almeida, H. P. da Silva, and A. Oliveira, "Design and evaluation of a novel approach to invisible electrocardiography (ecg) in sanitary facilities using polymeric electrodes," *Scientific Reports*, vol. 11, p. 6222, 12 2021. [Online]. Available: http://www.nature.com/articles/s41598-021-85697-2

[15] Y. Meng, Z. B. Li, X. Chen, and J. P. Chen, "A flexible dry micro-dome electrode for ecg monitoring," *Microsystem Technologies*, vol. 21, pp. 1241–1248, 6 2015.

[16] T. H. Kim, C. Bao, Z. Chen, and W. S. Kim, "3d printed leech-inspired origami dry electrodes for electrophysiology sensing robots," *npj Flexible Electronics*, vol. 6, 12 2022.

[17] P. Salvo, R. Raedt, E. Carrette, D. Schaubroeck, J. Vanfleteren, and L. Cardon, "A 3d printed dry electrode for ecg/eeg recording," *Sensors and Actuators A: Physical*, vol. 174, pp. 96–102, 2 2012.

[18] "Single-lead, heart rate monitror front end," *ANALOG DEVICES*.

[19] "Arduino® uno r3," *ARDUINO*.

[20] "2021 asus tuf dash f15laptops for gamingasus global." [Online]. Available: https://www.asus.com/Laptops/For-Gaming/TUF-Gaming/2021-ASUS-TUF-Dash-F15/

[21] M. Cadogan, "Ecg lead positioning • litfl • ecg library basics." [Online]. Available: https://litfl.com/ecg-lead-positioning/

[22] J. Machiels, A. Verma, R. Appeltans, M. Buntinx, E. Ferraris, and W. Deferme, "Printed Electronics (PE) As An enabling Technology to Realize Flexible Mass Customized Smart Applications," *Procedia CIRP*, vol. 96, pp. 115–120, 2020. [Online]. Available: https://doi.org/10.1016/j.procir.2021.01.062

[23] N. Meziane, J. G. Webster, M. Attari, and A. J. Nimunkar, "Dry electrodes for electrocardiography," *Physiological Measurement*, vol. 34, no. 9, 2013.

[24] R. Dorey, "Integration and devices: What type of structures are required for thick-film devices, why is it difficult to make them, and how can the challenges be overcome?" *Ceramic Thick Films for MEMS and Microdevices*, pp. 1–33, jan 2012.

[25] S. J. Cho, D. Byun, T. S. Nam, S. Y. Choi, B. G. Lee, M. K. Kim, and S. Kim, "A 3D-Printed Sensor for Monitoring Biosignals in Small Animals," *Journal of Healthcare Engineering*, vol. 2017, 2017.

[26] A. Ghilan, · . Aurica, P. Chiriac, · . Loredana, E. Nita, A. G. Rusu, I. Neamtu, · . Vlad, and M. Chiriac, "Trends in 3D Printing Processes for Biomedical Field: Opportunities and Challenges," vol. 28, pp. 1345–1367, 2020. [Online]. Available: https://doi.org/10.1007/s10924-020-01722-x

[27] C. K. Chua, W. Y. Yeong, and J. An, "Special Issue: 3D Printing for Biomedical Engineering," *Materials*, vol. 10, no. 3, 2017. [Online]. Available: /pmc/articles/PMC5503334//pmc/articles/PMC5503334/?report= abstracthttps://www.ncbi.nlm.nih.gov/pmc/articles/PMC5503334/

[28] C. L. Ventola, "Medical Applications for 3D Printing: Current and Projected Uses." vol. 39, no. 10, pp. 704–711, 2014. [Online]. Available: http://www.ncbi.nlm.nih.gov/pubmed/25336867%5

[29] A. Kalkal, S. Kumar, P. Kumar, R. Pradhan, M. Willander, G. Packirisamy, S. Kumar, and B. D. Malhotra, "Recent advances in 3D printing technologies for wearable (bio)sensors," *Additive Manufacturing*, vol. 46, p. 102088, oct 2021.

[30] Ashish, N. Ahmad, P. Gopinath, and A. Vinogradov, "3D Printing in Medicine: Current Challenges and Potential Applications," *3D Printing Technology in Nanomedicine*, pp. 1–22, jan 2019.

[31] M. Schouten, G. Wolterink, A. Dijkshoorn, D. Kosmas, S. Stramigioli, and G. Krijnen, "A Review of Extrusion-Based 3D Printing for the Fabrication of Electro- A nd Biomechanical Sensors," *IEEE Sensors Journal*, vol. 21, no. 11, pp. 12 900–12 912, jun 2021.

[32] R. E. Gregg, S. H. Zhou, J. M. Lindauer, E. D. Helfenbein, and K. K. Giuliano, "What is inside the electrocardiograph?" *Journal of Electrocardiology*, vol. 41, no. 1, pp. 8–14, 2008.

[33] J. L. Salinet and O. Luppi Silva, "ECG Signal Acquisition Systems," *Developments and Applications for ECG Signal Processing: Modeling, Segmentation, and Pattern Recognition*, pp. 29–51, jan 2019.

[34] A. C. Deswysen, E. Zimerson, A. Goossens, M. Bruze, and M. Baeck, "Allergic contact dermatitis caused by self-adhesive electrocardiography electrodes in an infant," *Contact Dermatitis*, vol. 69, no. 6, pp. 379–381, dec 2013. [Online]. Available: https://onlinelibrary.wiley.com/doi/full/10.1111/cod.12137https://onlinelibrary.wiley.com/doi/abs/10.1111/cod.12137https://onlinelibrary.wiley.com/doi/10.1111/cod.12137

[35] M. A. Lopez-Gordo, D. S. Morillo, and F. P. Valle, "Dry eeg electrodes," *Sensors 2014, Vol. 14, Pages 12847-12870*, vol. 14, pp. 12 847–12 870, 7 2014. [Online]. Available: https://www.mdpi.com/1424-8220/14/7/12847/htmhttps://www.mdpi.com/1424-8220/14/7/12847

[36] "Electrifi faqs." [Online]. Available: https://www.multi3dllc.com/faqs/

[37] D. G. Nicholls and S. Ferguson, "Bioenergetics: Fourth edition," *Bioenergetics: Fourth Edition*, pp. 1–419, 7 2013.

[38] A. K. B. M. M. S. D. B. E. STROUD and B. D. P. Mitchell, "Coupling of phosphorylation to electron and hydrogen transfer by a chemi-osmotic type of mechanism," *Nature 1961 191:4784*, vol. 191, pp. 144–148, 1961. [Online]. Available: https://www.nature.com/articles/191144a0

[39] J. M. Benarroch and M. Asally, "The microbiologist's guide to membrane potential dynamics," *Trends in microbiology*, vol. 28, pp. 304–314, 4 2020. [Online]. Available: https://pubmed.ncbi.nlm.nih.gov/31952908/

[40] J. Norbert, "Transmembrane ionic currents underlying cardiac action potential in mammalian hearts," *Advances in Cardiomyocyte Research*, pp. 1–45, 2009. [Online]. Available: https://www.researchgate.net/publication/249962676_Transmembrane_ionic_currents_underlying_cardiac_action_potential_in_mammalian_hearts

[41] D. A. McCormick, "Membrane potential and action potential," *From Molecules to Networks: An Introduction to Cellular and Molecular Neuroscience: Third Edition*, pp. 351–376, 1 2014.

[42] P. Y, J. R, and A. NR, "Physiology, sodium potassium pump," *StatPearls*, 2 2019. [Online]. Available: http://europepmc.org/books/NBK537088https://europepmc.org/article/med/30725773

[43] J. R. Schofield, "Electrocardiogram signal quality comparison between a dry electrode and a standard wet electrode over a period of extended wear." [Online]. Available: https://engagedscholarship.csuohio.edu/etdarchive

[44] M. Vaz, A. Kurpad, and T. Raj, "Guyton and hall textbook of medical physiology-3rd sae (third south asian edition)."

[45] "Health library, diagnostic and testing, url=https://my.clevelandclinic.org, journal=Cleveland Clinic."

[46] "Target heart rates chart, url=https://www.heart.org/en/healthy-living/fitness/fitness-basics/target-heart-rates, journal=American Heart Association."

[47] D. M. Krikler, "Electrocardiography then and now: where next?" *British Heart Journal*, vol. 57, p. 113, 1987. [Online]. Available: https://www.ncbi.nlm.nih.gov/pmc/articles/PMC1277090/

[48] C. Fisch, "Evolution of the clinical electrocardiogram," *Journal of the American College of Cardiology*, vol. 14, pp. 1127–1138, 11 1989. [Online]. Available: https://pubmed.ncbi.nlm.nih.gov/2681318/

[49] S. S. Barold, "Willem einthoven and the birth of clinical electrocardiography a hundred years ago," *Cardiac Electrophysiology Review*, vol. 7, pp. 99–104, 2003.

[50] H. J. J. Wellens, F. W. H. M. Bär, and K. I. Lie, "The value of the electrocardiogram in the differential diagnosis of a tachycardia with a widened qrs complex," *Professor Hein J.J. Wellens: 33 Years of Cardiology and Arrhythmology*, pp. 173–181, 2000. [Online]. Available: https://link.springer.com/chapter/10.1007/978-94-011-4110-9_17

[51] P. J. Zimetbaum and M. E. Josephson, "Use of the electrocardiogram in acute myocardial infarction," *http://dx.doi.org/10.1056/NEJMra022700*, vol. 348, pp. 933–940, 10 2009. [Online]. Available: https://www.nejm.org/doi/full/10.1056/nejmra022700

[52] E. B. Sgarbossa, Y. Birnbaum, and J. E. Parrillo, "Electrocardiographic diagnosis of acute myocardial infarction: Current concepts for the clinician," *American Heart Journal*, vol. 141, pp. 507–517, 4 2001.

[53] P. O. Ettinger, T. J. Regan, and H. A. Oldewurtel, "Hyperkalemia, cardiac conduction, and the electrocardiogram: A review," *American Heart Journal*, vol. 88, pp. 360–371, 9 1974.

[54] E. H. Houssein, M. Kilany, and A. E. Hassanien, "Ecg signals classification: a review," *International Journal of Intelligent Engineering Informatics*, vol. 5, p. 376, 2017.

[55] A. EA and N. J, "Conquering the ecg - cardiology explained," 2004. [Online]. Available: https://www.ncbi.nlm.nih.gov/books/NBK2214/

[56] Y. Sattar and L. Chhabra, "Electrocardiogram," in *StatPearls [Internet].* StatPearls Publishing, 2021.

[57] M. A. Serhani, H. T. E. Kassabi, H. Ismail, and A. N. Navaz, "Ecg monitoring systems: Review, architecture, processes, and key challenges," *Sensors (Basel, Switzerland)*, vol. 20, 3 2020. [Online]. Available: /pmc/articles/PMC7147367//pmc/articles/PMC7147367/?report=abstracthttps://www.ncbi.nlm.nih.gov/pmc/articles/PMC7147367/

[58] H. Sohn, C. R. Farrar, F. M. Hemez, D. D. Shunk, D. W. Stinemates, B. R. Nadler, and J. J. Czarnecki, "A review of structural health monitoring literature: 1996–2001," *Los Alamos National Laboratory, USA*, vol. 1, 2003.

[59] H. Benhar, A. Idri, and J. L. Fernández-Alemán, "Data preprocessing for heart disease classification: A systematic literature review," *Computer Methods and Programs in Biomedicine*, vol. 195, p. 105635, 10 2020.

[60] J. S. Karnewar and V. K. Shandilya, "Preprocessing ecg signal by eliminating various noises using denoising methods," *AIP Conference Proceedings*, vol. 2424, p. 080003, 3 2022. [Online]. Available: https://aip.scitation.org/doi/abs/10.1063/5.0076807

[61] S. Karpagachelvi, M. Arthanari, and M. Sivakumar, "Ecg feature extraction techniques - a survey approach," 5 2010. [Online]. Available: https://arxiv.org/abs/1005.0957

[62] S. Chandra, A. Sharma, and G. K. Singh, "Feature extraction of ECG signal," *Journal of Medical Engineering & Technology*, vol. 42, no. 4, pp. 306–316, 2018. [Online]. Available: https://doi.org/10.1080/03091902.2018.1492039

[63] A. Gacek, "An introduction to ecg signal processing and analysis," *ECG Signal Processing, Classification and Interpretation: A Comprehensive Framework of Computational Intelligence*, vol. 9780857298683, pp. 21–46, 6 2014. [Online]. Available: https://link.springer.com/chapter/10.1007/978-0-85729-868-3_2

[64] R. R. Bond, D. D. Finlay, C. D. Nugent, G. Moore, and D. Guldenring, "Methods for presenting and visualising electrocardiographic data: From temporal signals to spatial imaging." *Journal of electrocardiology*, vol. 46, no. 3, pp. 182–196, 2013.

[65] M. Raeiatibanadkooki, S. R. Quachani, M. Khalilzade, and K. Bahaadinbeigy, "Real time processing and transferring ecg signal by a mobile phone," *Acta Informatica Medica*, vol. 22, p. 389, 2014. [Online]. Available: /pmc/articles/PMC4315648//pmc/articles/PMC4315648/?report= abstracthttps://www.ncbi.nlm.nih.gov/pmc/articles/PMC4315648/

[66] X. Zhai, A. Ait, and S. Ali, "Ecg encryption and identification based security solution on the zynq soc for connected health systems."

[67] R. L. Weinberg, "Standards for inpatient electrocardiographic monitoring - american college of cardiology," 10 2017. [Online]. Available: https://www.acc.org/latest-in-cardiology/ten-points-to-remember/2017/10/04/12/26/update-to-practice-standards-for-electrocardiographic-monitoring

[68] "12-Lead ECG Placement Guide with Illustrations." [Online]. Available: https://www.cablesandsensors.com/pages/12-lead-ecg-placement-guide-with-illustrations

[69] "12 lead placement guide with diagram." [Online]. Available: https://aimcardio.com/blog/12-lead-placement-guide-with-diagram/

[70] "Wet and dry electrodes for eeg - sapien labs — neuroscience — human brain diversity project." [Online]. Available: https://sapienlabs.org/lab-talk/wet-and-dry-electrodes-for-eeg/

[71] N. Shahrubudin, T. C. Lee, and R. Ramlan, "An overview on 3d printing technology: Technological, materials, and applications," *Procedia Manufacturing*, vol. 35, pp. 1286–1296, 2019.

[72] "Additive manufacturing - general principles - part 1: Terminology, url=https://www.iso.org/obp/ui/iso:std:iso:17296:-1:dis:ed-1:v1:en, journal=ISO/RF 17296."

[73] S. A. Tofail, E. P. Koumoulos, A. Bandyopadhyay, S. Bose, L. O'Donoghue, and C. Charitidis, "Additive manufacturing: scientific and technological challenges, market uptake and opportunities," *Materials Today*, vol. 21, pp. 22–37, 1 2018.

[74] C. Barnatt, "3D printing : the next industrial revolution," Charleston, S.C, 2013.

[75] ISO/ASTM, "Additive Manufacturing - General Principles Terminology (ASTM52900)," *Rapid Manufacturing Association*, pp. 10–12, 2013. [Online]. Available: http://www.ciri.org.nz/nzrma/technologies.html

[76] D. J. Braconnier, R. E. Jensen, and A. M. Peterson, "Processing parameter correlations in material extrusion additive manufacturing," *Additive Manufacturing*, vol. 31, p. 100924, 1 2020.

[77] J. W. Stansbury and M. J. Idacavage, "3d printing with polymers: Challenges among expanding options and opportunities," *Dental Materials*, vol. 32, pp. 54–64, 1 2016.

[78] "Layers and Perimeters." [Online]. Available: https://help.prusa3d.com/en/article/layers-and-perimeters_1748

[79] "What is the best print speed for 3D Printing." [Online]. Available: https://3dprinterly.com/best-print-speed-settings-for-3d-printing/

[80] P. Dudek, "FDM 3D printing technology in manufacturing composite elements," *Archives of Metallurgy and Materials*, vol. 58, no. 4, pp. 1415–1418, 2013.

[81] I. Blanco, "The use of composite materials in 3d printing," *Journal of Composites Science 2020, Vol. 4, Page 42*, vol. 4, p. 42, 4 2020. [Online]. Available: https://www.mdpi.com/2504-477X/4/2/42/htmhttps://www.mdpi.com/2504-477X/4/2/42

[82] X. Wang, M. Jiang, Z. Zhou, J. Gou, and D. Hui, "3d printing of polymer matrix composites: A review and prospective," *Composites Part B: Engineering*, vol. 110, pp. 442–458, 2 2017.

[83] I. Blanco, "The rediscovery of poss: A molecule rather than a filler," *Polymers 2018, Vol. 10, Page 904*, vol. 10, p. 904, 8 2018. [Online]. Available: https://www.mdpi.com/2073-4360/10/8/904/htmhttps://www.mdpi.com/2073-4360/10/8/904

[84] M. L. Shofner, K. Lozano, F. J. Rodríguez-Macías, and E. V. Barrera, "Nanofiber-reinforced polymers prepared by fused deposition modeling," *Journal of Applied Polymer Science*, vol. 89, pp. 3081–3090, 9 2003. [Online]. Available: https://onlinelibrary.wiley.com/doi/full/10.1002/app.12496https://onlinelibrary.wiley.com/doi/abs/10.1002/app.12496https://onlinelibrary.wiley.com/doi/10.1002/app.12496

[85] S. Singh, S. Ramakrishna, and F. Berto, "3d printing of polymer composites: A short review," *Material Design Processing Communications*, vol. 2, p. e97, 4 2020. [Online]. Available: https://onlinelibrary.wiley.com/doi/full/ 10.1002/mdp2.97https://onlinelibrary.wiley.com/doi/abs/10.1002/mdp2.97https: //onlinelibrary.wiley.com/doi/10.1002/mdp2.97

[86] R. L. Boylestad, *Introductory Circuit Analysis*, 10th ed.   USA: Prentice Hall PTR, 2002.

[87] R. F. Pierret, *Advanced Semiconductor Fundamentals*.   USA: Addison-Wesley Longman Publishing Co., Inc., 1987.

[88] H. S. Magar, R. Y. Hassan, and A. Mulchandani, "Electrochemical impedance spectroscopy (eis): Principles, construction, and biosensing applications," *Sensors (Basel, Switzerland)*, vol. 21, 10 2021. [Online]. Available: /pmc/articles/PMC8512860//pmc/articles/PMC8512860/?report= abstracthttps://www.ncbi.nlm.nih.gov/pmc/articles/PMC8512860/

[89] "Conductive silver epoxy kit, url=https://www.emsdiasum.com/microscopy/technic datasheet/12642-14.aspx, journal=Electron Microscopy Sciences."

[90] "3m ecg electrode." [Online]. Available: https://www.3m.com.ec/3M/es_EC/p/d/ v000183146/

[91] "Hydra 16a." [Online]. Available: https://hyrel3d.com/wiki/index.php/Hydra_16A

[92] "4200a-scs parameter analyzer." [Online]. Available: https://download.tek.com/ datasheet/1KW-60780-6_4200A-SCS_Parameter_Analyzer_Datasheet_120120.pdf

[93] "Semiprobe high frequency/microwave." [Online]. Available: https://www. semiprobe.com/applications/high-frequency-microwave/

[94] "Cd800a digital multimeter." [Online]. Available: https://www.sanwa-meter.co.jp/ japan/pdf/catalog/digital_multimeters/CD800a_EN_catalog.pdf

[95] "Palmsense4." [Online]. Available: https://www.palmsens.com/product/palmsens4/

[96] Z. Wang, C. Chen, W. Li, W. Yuan, T. Han, C. Sun, L. Tao, Y. Zhao, and W. Chen, "A Multichannel EEG Acquisition System with Novel Ag NWs/PDMS Flexible Dry Electrodes," *Proceedings of the Annual International Conference of the IEEE Engineering in Medicine and Biology Society, EMBS*, vol. 2018-July, no. 2017, pp. 1299–1302, 2018.

[97] "Electrically insulating plastics." [Online]. Available: https://www.ensingerplastics. com/en/shapes/plastic-material-selection/electrically-insulative

[98] "What is labview? graphical programming for test measurement - ni." [Online]. Available: https://www.ni.com/en-us/shop/labview.html

[99] Y. Wang, R. Wunderlich, and S. Heinen, "Design and evaluation of a novel wireless reconstructed 3-lead ecg monitoring system," pp. 362–365, 2013.

[100] R. Kusche, S. Kaufmann, and M. Ryschka, "Dry electrodes for bioimpedance measurements - Design, characterization and comparison," *Biomedical Physics and Engineering Express*, vol. 5, no. 1, 2019.

[101] S. Roy, M. B. Qureshi, S. Asif, and B. D. Braaten, *A Model for 3D-Printed Microstrip Transmission Lines using Conductive Electrifi Filament.* [Online]. Available: www.multi3dllc.com

[102] P. F. Flowers, C. Reyes, S. Ye, M. J. Kim, and B. J. Wiley, "3d printing electronic components and circuits with conductive thermoplastic filament," *Additive Manufacturing*, vol. 18, pp. 156–163, 12 2017.

[103] A. Albulbul and A. D. Chan, "Electrode-skin impedance changes due to an externally applied force," *MeMeA 2012 - 2012 IEEE Symposium on Medical Measurements and Applications, Proceedings*, pp. 61–64, 2012.

[104] E. J. Clar, C. P. Her, and C. G. Sturelle, "Skin impedance and moisturization in london at the ifscc viiith international congress on 'cosmetics-quality and safety' organized by the society of cosmetic chemists of great britain," *J. Soc. Cosmet. Chem*, vol. 26, pp. 337–353, 1975.